MINIATURE ENDPLATE POTENTIAL FREQUENCY AND AMPLITUDE DETERMINED BY AN EXTENSION OF CAMPBELL'S THEOREM

J. R. SEGAL,* B. CECCARELLI,‡ R. FESCE,§ AND W. P. HURLBUT§

*Biophysics Laboratory, Veterans Administration Medical Center, New York, New York 10010; and ‡Department of Pharmacology and Center for the Study of Peripheral Neuropathies and Neuromuscular Diseases, University of Milan; Consiglio Nazionale delle Richerche (CNR) Center of Cytopharmacology, 20129 Milano, Italy; and §The Rockefeller University, New York, New York 10021

ABSTRACT A method based upon an extension of Campbell's theorem is used to measure the amplitude, waveform, and frequency of occurrence of miniature endplate potentials (mepps) at rapidly secreting neuromuscular junctions of frog cutaneous pectoris muscles. Measurements of the variance, skew, and power spectrum of the fluctuations in membrane potential are used to deduce the mepp parameters. These estimates of mepp amplitude and frequency are insensitive to slow drifts in membrane potential that preclude the conventional application of Campbell's theorem, which uses the mean and variance. The new method becomes unreliable at high mepp frequencies because the distribution of the values of membrane potential approaches a Gaussian thereby reducing the accuracy of skew measurements. Frequencies approaching 10^4 s^{-1} can be measured, however, if the data are high-pass filtered. The method has been tested with computer simulated data and applied to junctions exposed to La^{3+}; the effects of Ca^{2+} on the La^{3+}-induced secretion have been explored. Some muscles were fixed after treatment with La^{3+}, and changes in nerve terminal ultrastructure were assessed by morphometric analysis of electron micrographs. Horseradish peroxidase was used to obtain information about vesicle recycling.

INTRODUCTION

Neurotransmitters are secreted from nerve terminals by two means (*a*) in multimolecular packets or quanta (del Castillo and Katz, 1956), and (*b*) by the "leakage" of individual molecules (Katz and Miledi, 1977). Quantal secretion produces readily observed changes in the electrical properties of the postsynaptic cells and generates the transient depolarizations that are responsible for synaptic transmission (del Castillo and Katz, 1956). At vertebrate neuromuscular junctions the transmitter is acetylcholine (ACh) and the secrection of each quantum is signaled by the occurrence of a miniature endplate potential (mepp), a brief, localized, stereotyped depolarization of the endplate region of the muscle fiber (Fatt and Katz, 1952). Nonquantal secretion, on the other hand, usually does not produce obvious electric effects in the postsynaptic cell, although under some conditions it may cause small, steady depolarizations at an endplate (Katz and Miledi, 1977).

Although the central role of quantal secretion in synaptic transmission is well established, the origin of quanta in the presynaptic cell is controversial. The vesicle hypothesis holds that each quantum is stored within a synaptic vesicle located within the axoplasm of the nerve terminal; it is released by exocytosis when the vesicle membrane fuses with the presynaptic membrane of the terminal (del Castillo and Katz, 1956; Ceccarelli et al., 1979*a*,*b*; Heuser et al., 1979). If this were true, then the number of synaptic vesicles in a terminal should decline when the terminal secretes quanta, unless the vesicles that have fused with the axolemma are replaced. Large reductions in the numbers of synaptic vesicles in secreting terminals usually occur only after long periods of intense stimulation, and then the loss of vesicles is generally inadequate to account for the estimated number of quanta secreted. Since the rate of endocytosis is also increased at rapidly secreting terminals (Holtzman et al., 1971; Ceccarelli et al., 1972; Heuser and Reese, 1973), it has been suggested that the vesicle population is sustained in these terminals by reforming vesicles from membrane that is recovered from the axolemma. This recycling hypothesis is supported by many observations (Ceccarelli and Hurlbut, 1980*b*), but alternative explanations of the observations have been proposed (Tauc, 1982).

Characterization of the recycling process during vigorous release requires a method that allows mepp amplitude and frequency to be measured when the mepps overlap so extensively that their individual features cannot be resolved. Since mepps recorded at single neuromuscular

R. Fesce's permanent address is the Department of Pharmacology and Center for the Study of Peripheral Neuropathies and Neuromuscular Diseases, University of Milan; (CNR) Center of Cytopharmacology, 20129 Milano, Italy.

junctions form a relatively homogeneous population, their amplitude and frequency can be estimated in principle by applying Campbell's theorem (Campbell, 1909; Rice, 1944) to measurements of the mean, variance, and power spectrum of the fluctuating signal (Dodge et al., 1968; Wong and Knight, 1980; Simoneau et al., 1980; Heuser and Miledi, 1971; Katz and Miledi, 1972; Anderson and Stevens, 1973). Campbell's theorem assumes that the changes in mean potential and its fluctuations are due solely to the linear summation of randomly occurring unitary events. Unfortunately, during experiments of relatively long duration (several minutes to several hours), the membrane potential at the endplate of a muscle fiber can be changed by many factors other than the summation of mepps. These include (*a*) damage caused by the recording micropipette; (*b*) effects produced by the stimulating agent itself (e.g., high concentrations of K^+; (*c*) the redistribution of ions, particularly Cl^- (Katz and Miledi, 1972); (*d*) the accumulation of unhydrolyzed ACh in the synaptic cleft; (*e*) high rates of nonquantal secretion. When the conventional form of Campbell's theorem is used to estimate mepp amplitude and frequency, small changes in the mean potential due to any of these extraneous factors can produce errors of several hundred percent.

Rice's (1944) extension of Campbell's theorem to higher moments of the fluctuations provides a path to circumvent the intolerable bias errors that can be introduced by extraneous sources of depolarization. Specifically, the skew, variance, and power spectrum of the fluctuations in membrane potential can be used to estimate mepp amplitude, h, waveform, and frequency of occurrence, ξ. This new method has several advantages over the classical one employing the mean and variance. First, the estimates of h and ξ are insensitive to changes in mean potential occurring between sampling intervals. Second, because the fluctuations of the potential about its mean rarely exceed a few millivolts, the estimates of mepp parameters are less susceptible to errors arising from the voltage dependence of the driving force or membrane resistance (the so-called nonlinear summation of mepps), and the values of the mepp parameters determined for a particular data collection interval reflect the membrane characteristics prevailing during that same interval. Third, data can be high-pass filtered to hold the mean at zero, thereby minimizing the effects of nonstationarities (Appendix). The major disadvantage of the new method is that the resulting measures of h and ξ have larger random errors, and for this reason it is desirable to use the conventional approach whenever feasible.

We tested the method under ideal conditions by analyzing records generated by computer simulation and applied it to neuromuscular junctions of frog cutaneous pectoris muscles treated with La^{3+}. This ion causes massive increases in the rate of quantal secretion and large changes in mepp amplitude and time course (De Bassio et al., 1971; Heuser and Miledi, 1971; Kriebel and Flory, 1983). Some of these muscles were fixed and the ultrastructure of their nerve terminals examined in the electron microscope; in others, the uptake of horseradish peroxidase (HRP) was also followed. We explored the effect of Ca^{2+} on the La^{3+}-induced changes in mepp parameters, nerve terminal ultrastructure, and uptake of HRP in order to test previous evidence that Ca^{2+} is important to the ability of a terminal to sustain high rates of quantal secretion (Ceccarelli and Hurlbut, 1980*a*). A preliminary account of this work has been published as an abstract (Segal et al., 1983).

THEORY

Consider a fluctuating signal, $V(t)$, generated by the linear summation of randomly occurring unitary events, $hF(t)$, where h is a time independent amplitude factor and $F(t)$ is a nondimensional function of time. The extension of Campbell's theorem states that the nth semi-invariant, λ_n, of the probability density of V, $p(V)$, is (Rice, 1944)

$$\lambda_n = \xi h^n \int_{-\infty}^{+\infty} [F(t)]^n dt = \xi h^n I_n, \tag{1}$$

where ξ equals average frequency of occurrence of the events and $I_n = \int_{-\infty}^{+\infty} [F(t)]^n dt$. The first three semi-invariants are related to the central moments, m_n, of $p(V)$, by $\lambda_1 = m_1 = \overline{V} = \xi h I_1$, $\lambda_2 = m_2 = \overline{(V - \overline{V})^2} = \xi h^2 I_2$, and $\lambda_3 = m_3 = \overline{(V - \overline{V})^3} = \xi h^3 I_3$, where the bars indicate average values. At a neuromuscular junction V is the membrane potential of the endplate region of the muscle fiber and $hF(t)$ is the mepp. The latter can be represented (see Results) by

$$hF(t) = h(e^{-t/\theta_1} - e^{-t/\theta_2}), \tag{2}$$

where θ_1 equals the decay time constant and θ_2, the rise time constant. It then follows that

$$m_1 = \xi h I_1 = \xi h(\theta_1 - \theta_2), \tag{3}$$

$$m_2 = \xi h^2 I_2 = \xi h^2 \frac{(\theta_1 - \theta_2)^2}{2(\theta_1 + \theta_2)}, \tag{4}$$

and

$$m_3 = \xi h^3 I_3 = \xi h^3 \left[\frac{2(\beta - \alpha)^3}{3\alpha\beta(2\alpha + \beta)(2\beta + \alpha)}\right], \tag{5}$$

where $\alpha = 1/\theta_1$ and $\beta = 1/\theta_2$.

The expected (single-sided) spectral density of V, due to randomly occurring mepps is, for Fourier frequency, f (cf. Verveen and DeFelice, 1974)

$$S(f) = 2\xi h^2 \left[\frac{(\theta_1 - \theta_2)^2}{1 + 4\pi^2 f^2(\theta_1^2 + \theta_2^2) + 16\pi^4 f^4 \theta_1^2 \theta_2^2}\right], \{f \neq 0\}. \tag{6}$$

The two time constants, θ_1 and θ_2, can be obtained from graphs of $S(f)$ vs. f and, in principle, combined with any pair of the above moments to yield ξ and h. At an early stage of the study it became apparent that m_1 could not be used, because during long experiments the absolute value of V was changed by factors seemingly unrelated to the summation of mepps. These direct current (DC) shifts translate into high values of ξ and low values of h when m_1 is used in the calculations (Fig. 5 *C*). We therefore elected to use m_2 and m_3, each of which is insensitive to slow changes in V

that occur outside the sampling interval. The appropriate expressions for h and ξ are

$$h = \frac{m_3}{m_2} \cdot \frac{I_2}{I_3}, \tag{7}$$

$$\xi = \frac{(m_2)^3}{(m_3)^2} \cdot \frac{(I_3)^2}{(I_2)^3}. \tag{8}$$

The primary limitation to the usefulness of this technique is the increasing difficulty of measuring m_3 as ξ becomes large. According to the central limit theorem, when $\xi \to \infty$ the probability distribution of the fluctuations of V tends to a Gaussian and the skew becomes too small, relatively, to be reliably measured. The probability density of the deviations of membrane potential from the mean is given by (Rice, 1944)

$$p(v) \sim \frac{e^{-v^2/2\sigma^2}}{\sigma(2\pi)^{1/2}} + \frac{m_3}{3!\sigma^4(2\pi)^{1/2}}\left[\frac{v^3}{\sigma^3} - \frac{3v}{\sigma}\right]e^{-v^2/2\sigma^2} + R(v)e^{-v^2/2\sigma^2}, \tag{9}$$

where $v = V - \bar{V}$, $\sigma^2 = m_2 = \lambda_2$, and $R(v)$ is the sum of the remaining terms of the series. The three terms are of the order $\xi^{-1/2}$, ξ^{-1}, and $\xi^{-3/2}$, respectively, so that the last one can be ignored, to a first approximation, when the behavior of the distribution is examined at large ξ. The first term of the series, $G(v)$, is a Gaussian, and the second, $D(v)$, approximates the deviation of $p(v)$ from Gaussian. Thus, at high ξ, the skew of $p(v)$ is

$$\text{SKEW} = \int_{-\infty}^{+\infty} v^3 G(v)\mathrm{d}v + \int_{-\infty}^{+\infty} v^3 D(v)\mathrm{d}v. \tag{10}$$

In principle, only $D(v)$ contributes to SKEW since $G(v)$ is symmetric about $v = 0$. However, with any particular set of experimental data, contributions to the measured skew arise also from random deviations of the actual distribution from the expected distribution, $p(v)$. The magnitude of this random error is difficult to predict exactly, but it is related to the area under one side of the first integral, and the fractional random error in the measurement of the skew is related to the ratio

$$R = \frac{\int_0^{+\infty} v^3 G(v)\mathrm{d}v}{\int_0^{+\infty} v^3 D(v)\mathrm{d}v}. \tag{11}$$

The theoretical value of R^2 is

$$R^2 = (8/\pi)\frac{(m_2)^3}{(m_3)^2} = (8\xi/\pi)\frac{(I_2)^3}{(I_3)^2}. \tag{12}$$

Substituting Eqs. 4 and 5 into Eq. 12 yields

$$R^2 = (8/\pi)\left[\frac{9(1 + 2\alpha/\beta)^2(1 + \alpha/2\beta)^2}{8(1 + \alpha/\beta)^3}\right]\xi\theta_1. \tag{13}$$

Thus, the fractional random error in measurements of the skew increases as ξ increases. Errors in the estimates of ξ and h that are based upon the skew must also increase as ξ increases, and when they equal the mean the estimates will be meaningless. The value of ξ at which this occurs can be defined as ξ_u and the associated value of R defined as R_u. It is difficult to obtain an explicit expression for the magnitude of R_u, but it must depend upon sample size and rate, and its value can be determined empirically from the analysis of computer simulated records. This analysis shows that $\xi_u \sim 3{,}000\ s^{-1}$ when $\theta_1 = 10$ ms and $\theta_2 = 1.5$ ms (Results), and therefore R_u must be <10 for our sampling conditions. If this value of R_u is substituted into Eq. 12, it follows that the measurements of ξ will become meaningless whenever $(m_2)^3/(m_3)^3 > 40$.

Since ξ_u increases as θ_1 decreases (Eq. 13), it should be helpful to shorten the effective time course of the mepp by passing the data though a simple high-pass resistance-capacitance (RC) filter, for example. Such a filter, of time constant τ, transforms the time course of the mepp to $hF(t)'$, where

$$F(t)' = Be^{-\beta t} - Ae^{-\alpha t} - Ce^{-\lambda t}, \tag{14}$$

$$A = \alpha/(\lambda - \alpha), \quad \alpha = 1/\theta_1,$$

$$B = \beta/(\lambda - \beta), \quad \beta = 1/\theta_2,$$

and

$$C = \frac{\lambda(\beta - \alpha)}{(\lambda - \beta)(\lambda - \alpha)}, \quad \lambda = 1/\tau.$$

The three integrals $I'_n = \int_{-\infty}^{+\infty} + [F(t)']^n \mathrm{d}t$ for this modified waveform are $I'_1 = 0 = B/\beta - A/\alpha - C/\lambda$, $I'_2 = B^2/2\beta + A^2/2\alpha + C^2/2\lambda - 2AB/(\alpha + \beta) + 2AC/(\alpha + \lambda) - 2BC/(\beta + \lambda)$, and $I'_3 = B^3/3\beta - 3B^2A/(2\beta + \alpha) - 3B^2C/(2\beta + \lambda) - A^3/3\alpha + 3A^2B/(2\alpha + \beta) - 3A^2C/(2\alpha + \lambda) - C^3/3\lambda + 3C^2B/(2\lambda + \beta) - 3C^2A/(2\lambda + \alpha) + 6ABC/(\alpha + \beta + \lambda)$. The values of h and ξ are obtained from m'_2 and m'_3, the moments of the filtered data, using the formulae

$$h = (m'_3/m'_2)(I'_2/I'_3) \tag{15}$$

and

$$\xi = \frac{(m'_2)^3}{(m'_3)^2} \cdot \frac{(I'_3)^2}{(I'_2)^3}. \tag{16}$$

I'_2 and I'_3 are calculated from the known value of τ and the values of θ_1 and θ_2 extracted from the power spectra of unfiltered data.

For filtered data, ξ_u depends upon all three time constants and can be written (for $R = 10$) in the form $\xi_u = (100\pi/8)(1/\tau)f(\epsilon,\eta)$, where $\epsilon = \beta/\lambda = \tau/\theta_2$, and $\eta = \alpha/\lambda = \tau/\theta_1$.

The full expression for $f(\epsilon,\eta)$ is complex and not worth writing out explicitly. For simulated data ($\theta_1 = 10$ ms, $\theta_2 = 1.5$ ms, $\tau = 3$ ms), $f(\epsilon,\eta) = 0.42$ and $\xi_u = 4{,}900\ s^{-1}$, an increase of ~60% over ξ_u for unfiltered simulated data. Experimental data were usually analyzed by setting τ to ~3.3 ms, a value about twice θ_2 and one-half θ_1. The value of $f(\epsilon,\eta)$ for $\epsilon = 2$ and $\eta = 0.5$ is 0.36 and ξ_u is ~4,300 s^{-1}. Some limiting values for ξ_u are $f(\epsilon,0.5) \to 1.08$ as $\theta_2 \to 0$ and $\xi_u \to 12{,}800\ s^{-1}$; $f(2,\eta) \to 0.48$ as $\theta_1 \to \infty$ and $\xi_u \to 5{,}900\ s^{-1}$.

MATERIALS AND METHODS

Electrophysiology

Pairs of cutaneous pectoris muscles were dissected from frogs, *Rana pipiens*, and mounted in Lucite chambers that held ~3 ml of bathing solution. Endplate regions of the muscle fibers were impaled with glass micropipettes filled with 3 M KCl (resistances 10–30 MΩ) and the membrane potential recorded with a conventional high-input impedance amplifier. The output of the amplifier was stored with an FM magnetic tape recorder (Tandberg Instrumentation Recorder, series 115; Tandbergs Radiofabrikk, A/S, Oslo, Norway or model 3964A; Hewlett-Packard Co., Palo Alto, CA) both as a record with a bandwidth of DC-1250 Hz and as a high gain alternating current (AC) one at 0.16–1,250 Hz.

Most experiments were conducted at room temperature, which varied by less than ±1°C during the course of a day but ranged from 16–24°C over the course of a year. In a few experiments the chamber was mounted on a Peltier device and cooled to 2–3°C. Changes in the bathing fluid were made with previously chilled solutions so that the temperature of the muscle bath remained below 3°C.

Solutions

The muscles were always mounted in a Ringer's solution containing: Na^+, 116 mM; K^+, 2.1 mM; Ca^{2+}, 1.8 mM; Cl^-, 117 mM; HPO_4^{2-}, 2 mM; $H_2PO_4^-$, 1 mM; pH 7.0. It was then replaced by a Tris-buffered (6 mM, pH 7.2) Ringer's solution that also contained 4 mM Mg^{2+}, when the effect of La^{3+} was to be tested. We used the lowest concentrations of La^{3+} that consistently caused large increases in mepp frequency: 0.1 mM at temperatures above 20°C (summer and fall), 0.2 mM at 16–17°C (winter), and 1.0 mM at 2–3°C. The effects of Ca^{2+} were usually determined with pairs of muscles from the same frog: one muscle was treated with a solution that contained La^{3+}, 4 mM Mg^{2+}, and 1.8 mM Ca^{2+}; the other muscle was exposed to the same concentrations of La^{3+} and Mg^{2+} and no added Ca^{2+}. Some of the latter muscles were first soaked for ~10 min in a Ca^{2+}-free solution with 1 mM ethylene glycol-bis-(β-aminoethyl ether)*N,N'*-tetra-acetic acid (EGTA) and 4 mM Mg^{2+}. The EGTA was removed 10–15 min before the La^{3+} was applied. This pretreatment did not appear to influence the results.

Computations

Tape recordings of the data were analyzed with a digital computer (11/23; Digital Equipment Corp., Marlboro, MA). Data were first passed though a low-pass Butterworth filter set at 1,250 Hz to prevent aliasing (model APVL-44-5; A. P. Circut Corp., New York or model 901F; Frequency Devices, Inc. Haverhill, MA). This signal (referred to as unfiltered) was then passed through a high-pass RC filter (time constant 3.1–3.4 ms for experiments at room temperature and 9.0 ms for experiments at 3°C) to obtain filtered data. Filtered or unfiltered data were sampled at 2,500 Hz (25,000 12-bit samples) and stored within the computer as an amplitude histogram from which m_2 and m_3 or m_2' and m_3' were computed. The computation required ~5 s, so ⅓ of the record was wasted. The moments were collected in groups of three and averaged to reduce random errors; the average values of the baseline moments, obtained from data collected at the beginning of an experiment before the addition of stimulants, were subtracted. The result was employed to calculate ξ and h only when the value of each moment exceeded either twice its average baseline value, or the baseline value plus twice its standard deviation, whichever was larger. Since the baseline records included some mepps, the reported values of ξ represent increments above the small resting level of ~1 s^{-1}. The average baseline moments were $m_2 = 1.1 \times 10^{-2}$ mV^2, $m_3 = 0.2 \times 10^{-3}$ mV^3 (unfiltered data); $m_2' = 0.7 \times 10^{-3}$ mV^2, $m_3' = 0.4 \times 10^{-4}$ mV^3 (filtered data). The average parameters of the control mepps were $h = 0.7$ mV, $\theta_1 = 5.2$ ms, and $\theta_2 = 1.0$ ms (Table II, Results). Thus, the smallest increase in ξ above the baseline that could be measured was ~10 s^{-1}.

The two time constants of the mepp were calculated from power spectra of unfiltered data computed by standard techniques (Bendat and Piersol, 1971) at intervals throughout each experiment. Two independent spectra were obtained from overlapping sets of data: 2,048 12-bit data points were collected at 500 Hz for one of these spectra (range: 0.25–250 Hz, 4-s sample) and at 2,500 Hz for the second (range: 1.25–1,250 Hz, 0.8-s sample). The signals were passed through the Butterworth low-pass filter set at one-half the respective sampling frequency, the ends of the records were cosine tapered, and a fast Fourier transform performed. The resultant power spectra were averaged in groups of eight and then smoothed further by frequency averaging. The overall smoothing was such that the theoretical normalized standard error ranged from 20% within the lowest frequency decade to 6.6% within the highest. This error is calculated as $(8L)^{-1/2}$, where L is the number of neighboring frequency components that are averaged (Bendat and Piersol, 1971). Baseline spectra, obtained from data recorded during the control period, were subtracted from the spectra obtained during stimulated secretion. A montage was made of the two final spectra, and θ_1 and θ_2 were computed from the half-power (f_1) and 10^{-4} power (f_u) frequencies using the approximations: $4\pi^2 f_1^2(\theta_1^2 + \theta_2^2) = 1$ and $4\pi^2 f_u^2(\theta_1\theta_2) = 100$. Derived from Eq. 6, they provide valid measures of θ_1 and θ_2 (<5% error) when $\theta_1 > 5\theta_2$, as is the case for the mepps. The ratios, I_2'/I_3' and $(I_2')^3/(I_3')^2$ were calculated from the known value of τ and the values of θ_1 and θ_2 determined from power spectra measured at various times during an experiment; combined with the measured moments, they yield h and ξ. The appropriate I_n and I_n' factors for other times were calculated from values of θ_1 and θ_2 obtained by linear interpolation between the measured ones.

Computer Simulation

The accuracy of the method, particularly with regard to the prediction of an upper limit to measures of mepp frequency, ξ_u, was tested by applying the technique to computer generated random sequences of mepps. For a given mean frequency, ξ, a Poisson random-number generator determined the number of events starting within a given 0.2-ms interval, and for every such event the computer generated 300 points of the mepp waveform described by Eq. 2 (unfiltered data) or by h times Eq. 14 (filtered data); 51 contiguous records, each consisting of 1,000 points simulating an interval 0.2 s in duration, were created by the linear temporal summation of the individual waveforms. The first of these records was discarded to avoid the effect of the initial transient, and the moments of the remainder were computed as described for real data. Single values of ξ and h were calculated from the average variance and skew of three independently simulated 10-s records. The procedure was repeated 10 times for each simulated frequency. The means and standard deviations of the resulting 10 estimates of ξ, h, and the moments were computed.

Parameters of Individual Mepps According to Eq. 2

The computer sampled recorded data at 0.2-ms intervals, stored 2,048 12-bit data points, and displayed them on a storage oscilloscope. Records containing isolated mepps were analyzed as follows. A mepp-free portion of the record was selected, its values averaged, and the logarithms of the deviations from this average were displayed. The declining phase of the mepps was usually exponential, i.e., linear on the semi-logarithmic display over most of its range. The slope and intercept of the exponential decay were determined by a least-squares fit to give θ_1 and h. The rise time constant, θ_2, was then calculated from t_p, the time-to-peak of the mepp, using the equation $1/\theta_2 = (1/t_p)\ln(\theta_1/\theta_2) + 1/\theta_1$. About 10 mepps were analyzed for each experimental condition.

Morphology

Both control and La^{3+}-treated muscles were fixed in the recording chambers for 1 h with a cold (4°C) solution of 2% OsO_4 in 0.1 M phosphate buffer, pH 7.3. Small specimens of tissue suspected to contain endplate regions were dissected out, and some of the specimens were block-stained with uranyl acetate. All specimens were dehydrated and then flat-embedded in EPON 812 (Ladd Research, Inc., Burlington, VT) according to standard procedures (Ceccarelli et al., 1972, 1973). Silver-gray sections were cut on a Reichert-Jung Ultracut microtome (C. Reichert Optische Werk AG, Vienna, Austria), double-stained with uranyl acetate and lead citrate, and examined in an electron microscope (H600; Hitachi Ltd., Tokyo, Japan).

Peroxidase

Muscles were incubated in the recording chambers for 0.5 h in Tris-buffered Ringer's solution that contained 4 mM Mg^{2+} and either 1.8 or 0 mM Ca^{2+}, and then for another hour in modified solutions that also contained 1.6% HRP (Sigma type VI; Sigma Chemical Co., St. Louis, MO) and 0.75% whale sperm myoglobin (Sigma type II; Sigma Chemical Co.). The bathing solution containing the extracellular tracers was then withdrawn, La^{3+} was added to a final concentration of 100 μM, and the resulting solution was reapplied to the muscle for an additional 0.5 h. We recorded intracellularly near single endplates throughout these incuba-

tions and monitored mepp frequency. It remained low during the preliminary incubation with extracellular tracers and rose to the usual high levels after La^{3+} had been added. The muscles were fixed with a solution containing 1% glutaraldehyde, 0.25% formaldehyde (freshly prepared from paraformaldehyde), and 0.1 M phosphate buffer, pH 7.3. Small pieces of muscle were removed, treated to reveal the sites of peroxidase activity, and processed further as described previously (Ceccarelli et al., 1973; Ceccarelli and Hurlbut, 1975, 1980*a*).

Morphometry

Electron micrographs were printed at a final magnification of 40,000, and the number, perimeter, and cross-sectional area of selected structures on the prints were determined with a Zeiss MOP 1 quantitative digital image analyzer (Carl Zeiss, Inc., Munich, Federal Republic of Germany). Only longitudinal sections of nerve terminals were examined. The following parameters were measured: (*a*) length of nerve terminal axolemma, (*b*) area of nerve terminal axoplasm, (*c*) number of synaptic vesicles, i.e., vesicular structures with diameters up to 50 nm, and coated vesicles, (*d*) number and total perimeter of large vesicular structures, i.e., vesicular structures with diameters >100 nm, (*e*) number and total length of infoldings, and (*f*) number of junctional folds (equals the number of active zones). Results are reported as mean values ± SD.

RESULTS

Simulated Data

Fig. 1 shows the results of applying our method to computer simulated data. All the moments rise linearly with ξ as described by Eqs. 4 and 5. The deviations of m_2 and m_2' from their theoretical values are very slight. This is not the case, however, for m_3 and m_3': their fractional standard deviations rise with ξ. The effect of these errors is

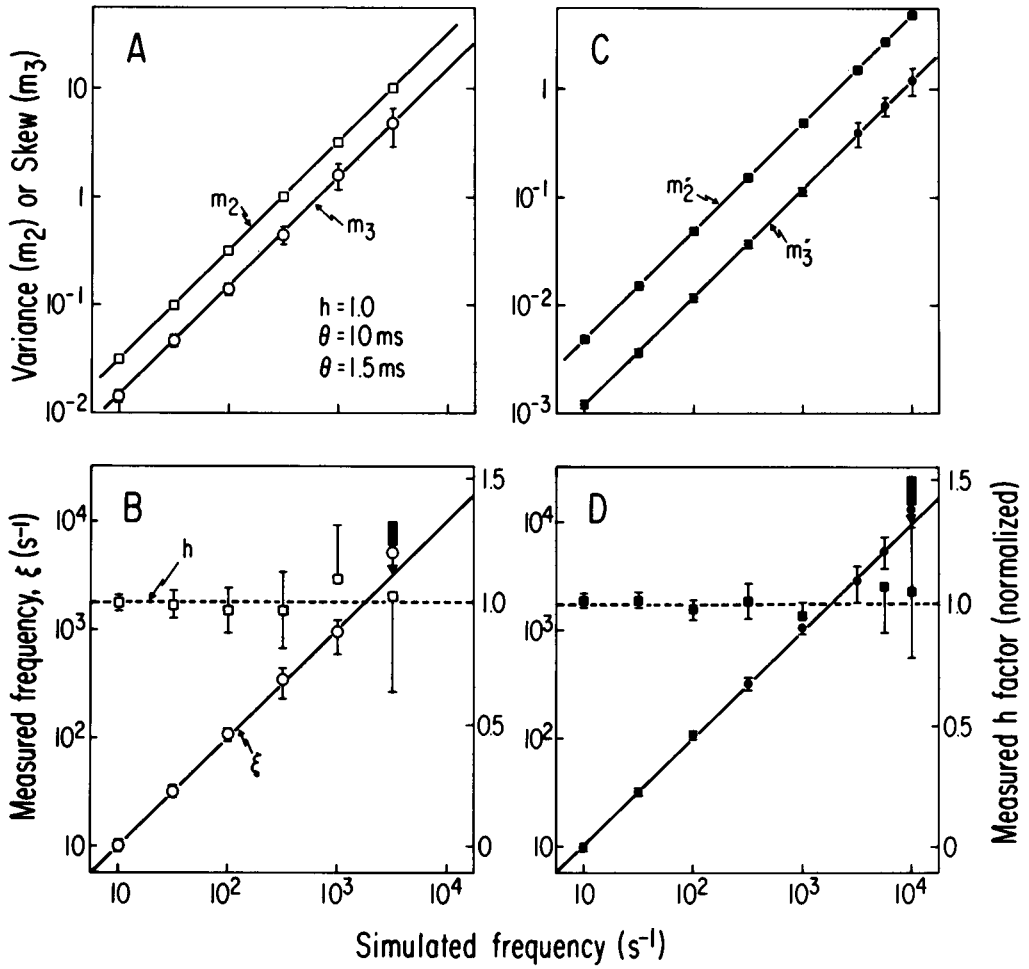

FIGURE 1 Results of the analysis of a fluctuating signal produced by computer simulation of mepps of known amplitude, time course, and mean frequency of occurrence. (*A* and *B*) unfiltered mepps; $h = 1$, $\theta_1 = 10$ ms, and $\theta_2 = 1.5$ ms; (*C* and *D*) filtered mepps; $h = 1$, $\theta_1 = 10$ ms, $\theta_2 = 1.5$ ms, and $\tau = 3.0$ ms. *Abscissae*: all graphs, mean frequency of randomly generated mepps. *Ordinates*: *A* and *C*, variance (squares) and skew (circles) of the fluctuations (log scale); *B* and *D*, frequency (circles, log scale) and *h* factor (squares, linear scale) computed from the skew and variance of the fluctuations as described in Methods. Mean values ±SD (bars). The broad bars and downward arrows at the highest frequencies indicate that the SD equals (or exceeds) the mean. The solid lines indicate the theoretical expected values of the variance, skew, and frequency. The dashed line is the theoretical value of *h*. At all ξ the means and variances of the simulated data are well behaved with SDs (bars) smaller than the sizes of the symbols in the graph.

amplified in the calculations of ξ, which require $(m_3)^2$ and $(m_3)^2$, so that with unfiltered data at 3,160 s^{-1} the standard deviation of the measured ξ is about equal to its mean. Because h depends linearly upon m_3 or m'_3, the errors in its measurement are considerably smaller and valid data can be obtained at higher frequencies. The salutary effect of high-pass filtering is evident from the results of Figs. 1 *C* and *D*. The fractional standard deviations of m'_3 are smaller than those of m_3, leading to smaller errors in the calculated values of ξ and h. With filtering ξ must rise to $\sim 10^4$ s^{-1} before its fractional standard deviation equals 1. Again, accurate values of h can be obtained at higher ξ. If we use the reasonable criterion that ξ must exceed its standard deviation in order to be measured reliably, it then follows that the theoretical upper limit, ξ_u, is well approximated by requiring $R < 10$ (Theory). These simulations show that reliable measurements can be made at La^{3+}-treated junctions when ξ does not exceed ~3,000 s^{-1} without filtering or ~5,000 s^{-1} with filtering.

The derivation of Campbell's theorem and its extension assume that ξ is stationary. Since we are interested in situations in which ξ changes with time, it is important to examine the effect of such nonstationarities. As an example we simulated, for filtered data, the case of ξ increasing exponentially during data generation. The simulation was of the somewhat extreme example of a 10-fold increase over a 40-s interval (corresponding to three 10-s periods of data collection separated by 5-s computation intervals). When $\bar{\xi}$ over the 40-s interval is 1,000 s^{-1} (midpoint frequency, $\xi_c = 809$ s^{-1}) and $h = 1$, the measured values of $\bar{\xi}$ and h are 999 ± 231 s^{-1} and 1.02 ± 0.12, respectively. When $\bar{\xi}$ is 3,160 s^{-1} ($\xi_c = 2{,}557$ s^{-1}), the measured $\bar{\xi}$ and h are 4,128 ± 1,594 s^{-1} and 0.983 ± 0.183, respectively. In the former case the values are reasonably accurate, but in

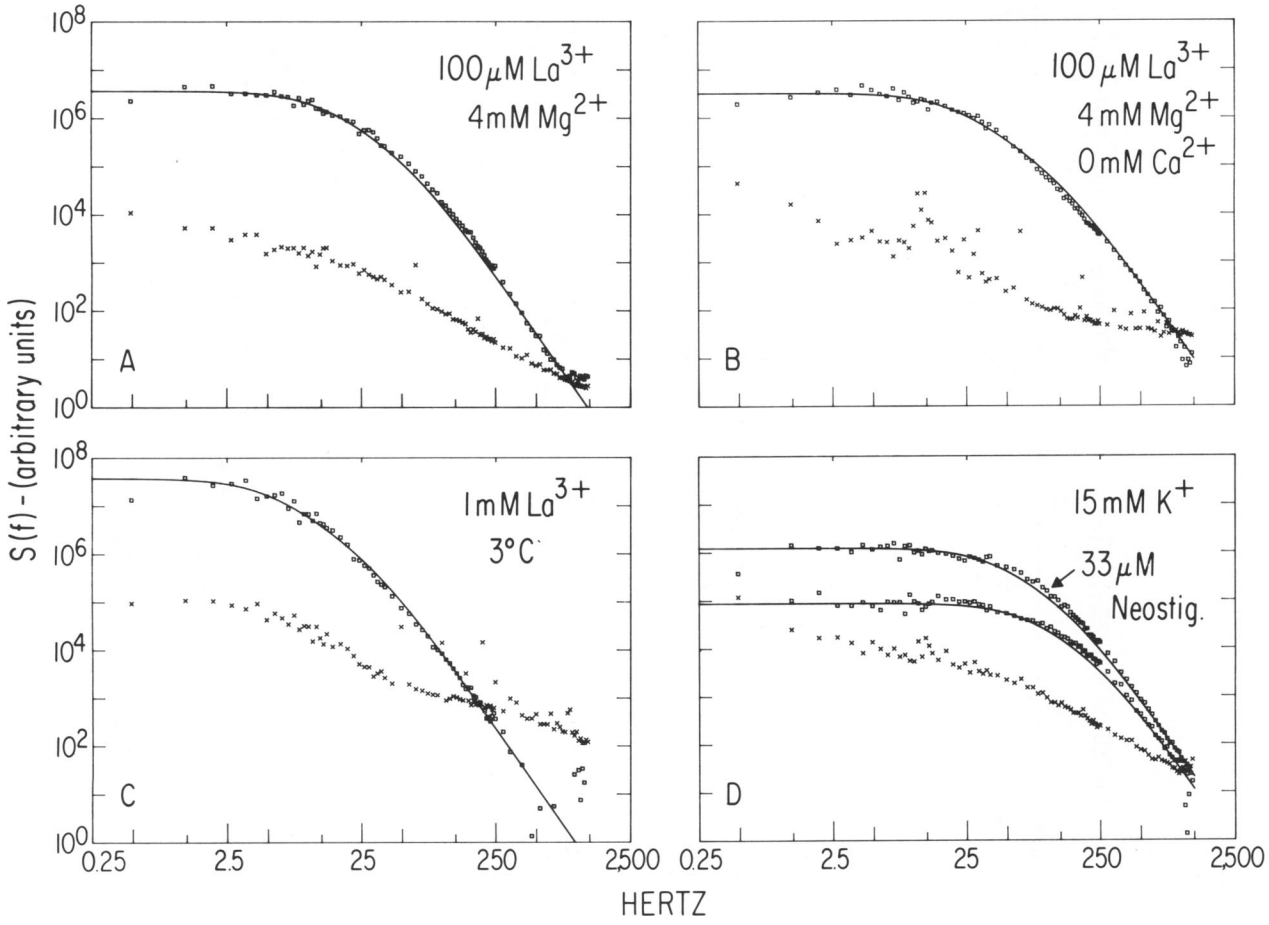

FIGURE 2 Power spectra of the fluctuations in membrane potential at rapidly secreting neuromuscular junctions. *Ordinates*: power per unit bandwidth (arbitrary units), log scale. *Abscissae*: frequency, hertz, log scale. The *lower* curve in each panel is the baseline spectrum (×), the other curve (□) is the difference between the spectrum obtained during rapid secretion and the baseline spectrum. The solid lines are theoretical curves drawn according to text Eq. 6 using values of θ_1 and θ_2 determined from the spectral points as described in the text. (*A*) Junction soaked for several minutes at 23°C in a modified Ringer's solution containing 100 μM La^{3+}, 1.8 mM Ca^{2+}, and 4 mM Mg^{2+}; θ_1 = 14.1 ms, θ_2 = 2.4 ms. (*B*) Junction soaked for several minutes at 22°C in a modified Ringer's solution containing 100 μM La^{3+}, 4 mM Mg^{2+}, and no Ca^{2+}; θ_1 = 9.0 ms, θ_2 = 1.0 ms. (*C*) Junction soaked for 15 min at 3°C in Ringer's solution with 1 mM La^{3+}; θ_1 = 35.5 ms, θ_2 = 4.6 ms is shown. (*D, middle* curve) Junction soaked 10 min in modified Ringer's solution containing 15 mM K^+; θ_1 = 2.53 ms, θ_2 = 0.54 ms; *top* curve: same junction several minutes after addition of 33 μM neostigmine; θ_1 = 4.45 ms, θ_2 = 0.88 ms. The first spectral points fall below the theoretical curves because the recording circuit was AC-coupled with a time constant of ~1 s.

the latter case the value of $\bar{\xi}$ is in error by ~30%. In this case, however, at the end of the 40-s interval ξ is at a level, 7,992 s^{-1}, which exceeds the limit of the technique. The method will be more accurate with the less drastic changes in ξ that actually occur experimentally during the data collection period. The results of the simulation are consistent with the theoretical analysis given in the Appendix.

Power Spectra of Active Endplates

Fig. 2 shows power spectra obtained from different junctions under a variety of experimental conditions: (*A*) 0.1 mM La^{3+} in Ringer's solution with 4 mM Mg^{2+} at 23°C, (*B*) 0.1 mM La^{3+} in a Ca^{2+}-free solution with 4 mM Mg^{2+} at 23°C, (*C*) 1 mM La^{3+} in Ringer's solution at 3°C, and (*D*) 15 mM K^+ or 15 mM K^+ plus 33 μM neostigmine. Solid curves are theoretical spectra of the form of Eq. 6. The deviations of the experimental data from them are within the theoretical limits of the accuracy with which the spectral points can be measured (Methods). Several important conclusions pertinent to the basic assumptions of the method follow from the conformity of the experimental spectra to Eq. 6. First, the fluctuations are due to the random, linear summation of independent unitary events of time course well represented by $F(t) = (e^{-t/\theta_1} - e^{-t/\theta_2})$. A different form for $F(t)$ would be reflected in the shape of the spectrum (Verveen and de Felice, 1974). Nonrandom or correlated occurrences of the mepps (clumping, for example) would produce recognizable components as additions to, or distortions of, the spectra described by Eq. 6 (Schick, 1974; Sigworth, 1981), as would nonlinear summation of the events. Second, the underlying events form a single population characterized by single mean values of θ_1 and θ_2. A bimodal population, for example, would produce a spectrum that is the sum of two different ones, each of the form of Eq. 6. Were this the case, it would not be possible to fit the data with a single pair of time constants, as has been done in Fig. 2. Third, the fluctuations measured during vigorous secretion are fully accounted for by the occurrence of mepps. Again, other sources of significant fluctuations would appear necessarily as modifications of the spectrum of Eq. 6. In sum, the close adherence of the data to Eq. 6 is strong evidence of the applicability of the assumptions underlying its derivation. Furthermore, the time constants derived from spectral analysis of active junctions change as expected: θ_1 and θ_2 are decreased by K^+ and are increased by neostigmine (Fatt and Katz, 1952, La^{3+} (Lambert and Parsons, 1970), and low temperature.

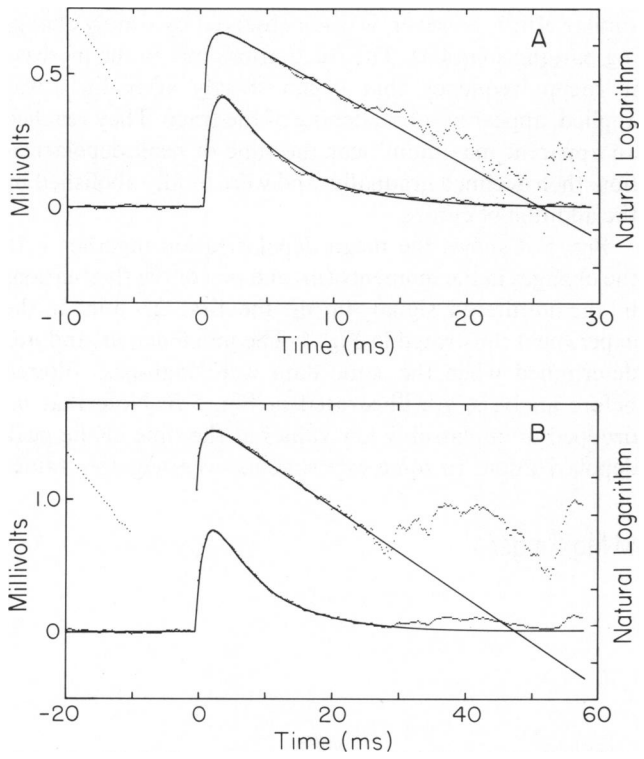

FIGURE 3 Comparison of the waveforms of the averaged mepp (dotted line) and the function: $h(e^{-t/\theta_1} - e^{-t/\theta_2})$ (solid line). *Ordinates*: millivolts (*left* axes), natural log (*right* axes). *Abscissae*: milliseconds. The lower pair of superimposed curves in each panel show the averaged and analytic mepp plotted on a linear scale. The upper pair of superimposed curves in each panel show these same data plotted on a log scale. The slope and intercept of the decay phase of the averaged mepp were used to determine θ_1 and h. The set of points near the upper-left corner of each panel is the function (he^{-t/θ_1} − averaged mepp) plotted on a log scale: θ_2 was calculated from the slope of this line and from the time-to-peak; the average of these values was used to construct the analytic curve. (*A*) Average of 21 superimposed mepps recorded near an endplate bathed in the Ca^{2+}-free control solution; θ_1 = 5.12 ms, θ_2 = 0.70 ms, h = 0.62 mV. (*B*) Average of 18 superimposed mepps recorded near the same endplate a few minutes after applying 100 μM La^{3+} but before the mepp frequency had risen above 50 s^{-1}. The unstable baseline beyond 30 ms is due to nonsuperimposed mepps; θ_1 = 8.39 ms, θ_2 = 1.28 ms, h = 1.26 mV. Note the differences in voltage and time scales of the two panels.

Waveform of Isolated Mepps

The analytic waveform that accounts for the power spectrum also describes well the shape of individual mepps when they are observable. Fig. 3 shows waveforms obtained by averaging 18–21 mepps recorded at a neuromuscular junction a few minutes before (*A*) and then a few minutes after (*B*) the addition of 100 μM La^{3+}, but before the mepp frequency had risen above 50 s^{-1}. The amplitude factor, h, and the time constants of decay, θ_1, and rise, θ_2, determined from this averaged waveform were used to construct the analytic curve: $F(t) = h(e^{-t/\theta_1} - e^{-t/\theta_2})$. This expression fits the average mepp in La^{3+} very well, deviating only slightly from the averaged control mepp at times <0.5 or beyond 10 ms.

Campbell's theorem and its extension do not make direct use of $F(t)$; they use instead either (*a*) the integral of the real mepp, J_1, of its square, J_2, or of its cube, J_3, or, more conveniently, (*b*) the factors, h^nI_n, computed analytically. Therefore, a better test of the adequacy of representing the mepp as the difference between two exponentials is to

TABLE I
MEPP PARAMETERS DETERMINED FROM SINGLE OR AVERAGED EVENTS

Parameter	Control (N = 21)		La^{3+} (N = 18)	
	Single	Averaged	Single	Averaged
θ_1 (ms)	5.30 ± 0.90	5.12	8.21 ± 2.36	8.39
θ_2 (ms)	0.79 ± 0.23	0.70	1.37 ± 0.33	1.28
h (mV)	0.66 ± 0.18	0.62	1.34 ± 0.26	1.26
I_1 (ms)	4.69 ± 1.05	4.56	6.78 ± 1.68	7.11
I_2 (ms)	1.88 ± 0.59	1.83	2.49 ± 0.99	2.62
I_3 (ms)	0.98 ± 0.40	0.94	1.16 ± 0.64	1.21
J_1^*(mV · ms)	2.82 ± 0.70	2.88	8.12 ± 1.95	8.50
hI_1/J_1‡	1.06 ± 0.033	0.97	1.07 ± 0.058	1.05
J_2^*(mV² · ms)	0.72 ± 0.026	0.69	4.22 ± 1.47	4.06
h^2I_2/J_2‡	1.06 ± 0.033	0.97	1.00 ± 0.081	1.02
J_3^*(mV³ · ms)	0.27 ± 0.15	0.22	2.68 ± 1.23	2.35
h^3I_3/J_3‡	0.98 ± 0.13	1.00	1.00 ± 0.12	1.03

*Empirical integrals of mepp.
‡Ratio: (theoretical integral)/(empirical integral).

compare the values of the factors, h^nI_n, calculated from the analytic curve, with the integrals, J_n, directly measured on individual or averaged mepps. The results of such a comparison are shown in Table I. The mean of the values determined from single mepps agrees within one standard error with the value determined from the averaged mepps, and the values determined from the individual or averaged mepps (J_n) agree very well with those determined from the analytic curve (h^nI_n). This analysis shows that for a population of mepps, albeit a limited one, no systematic errors are introduced by representing the real mepp as the difference between two exponentials. In any case, the application of Campbell's theorem is insensitive to the precise details of the individual waveforms, it being sufficient that the assumed average waveform accurately accounts for the average value of the above integrals.

Measurement of ξ and h

The strip chart recording of Fig. 4 illustrates the typical changes in membrane potential that occurred when 0.1 mM La^{3+} was applied in a solution with 4 mM Mg^{2+} and no added Ca^{2+}. The membrane potential began to decrease a few minutes after the La^{3+} was applied, reached a minimum at ~8 min, and then slowly increased over the next 40 min. An additional small increase occurred when a high concentration of curare was added at 55 min (a similar effect, however, is often observed by simply changing bathing solution). The fluctuations due to the increase in mepp frequency that began shortly after La^{3+} was applied, appear as a broadening of the trace. They reached an apparent maximum near the time of peak depolarization, then declined gradually, and were totally abolished by the addition of curare.

Fig. 5 *A* shows the mean depolarization together with the changes in the moments (m_2 and m_3) of the fluctuations in the unfiltered signal during the first 25 min of the experiment illustrated in Fig. 4. The moments, m_2' and m_3', determined when the same data were high-pass filtered before analysis, are illustrated in Fig. 5 *B*. Note that m_3 dropped to implausibly low values at the time of the peak depolarization. In some experiments even negative values

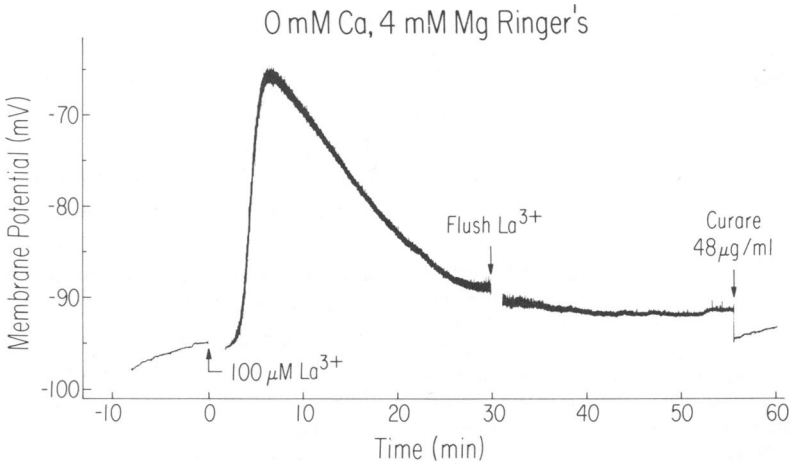

FIGURE 4 Effect of La^{3+} on the membrane potential of the endplate region of a muscle fiber bathed in a modified Ringer's solution with 4 mM Mg^{2+} and no Ca^{2+}. Chart recorder tracing. *Ordinate*: membrane potential (in millivolts). *Abscissa*: time after adding La^{3+}. The junction was impaled ~10 min before La^{3+} was applied; the initial resting potential was about −98 mV. The potential declined to about −95 mV during the baseline period. 100 μM La^{3+} was flushed in at zero time, causing a small hyperpolarization. The mepp frequency soon began to increase, thereby broadening of the trace. Membrane potential began to decrease after ~3 min, reached a minimum at ~8 min, and then slowly recovered. Fresh La^{3+} solution was flushed in at 30 min, causing another small hyperpolarization. Membrane potential remained fairly constant at about −90 mV for the next half hour, while mepp frequency gradually declined. A La^{3+} solution containing curare (48 μg/ml) was flushed in at 55 min, the fiber hyperpolarized slightly, the mepps vanished, and the trace became quiet.

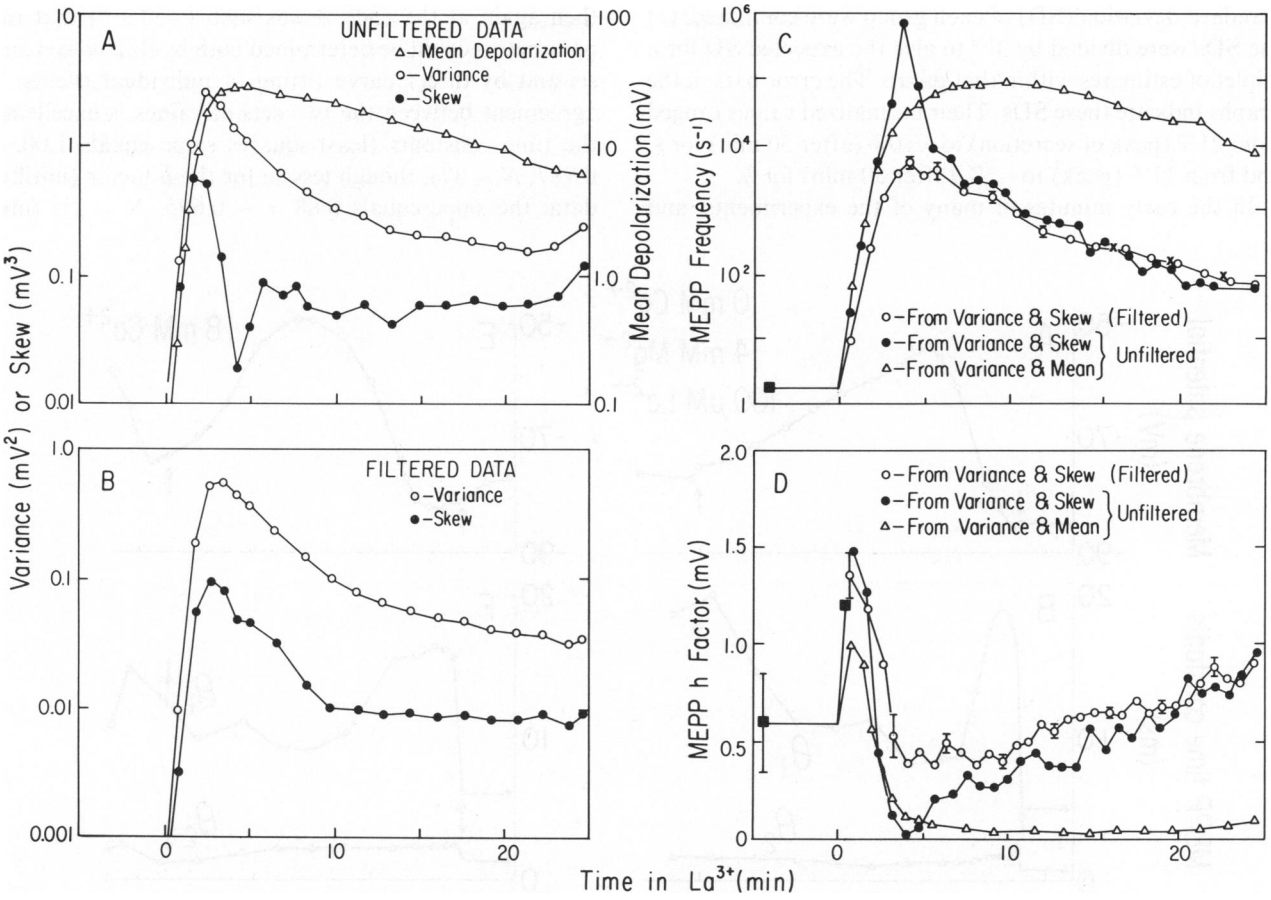

FIGURE 5 (*A* and *B*) Changes in mean membrane potential and variance and skew of its fluctuations during the first 25 min of the experiment illustrated in Fig. 4. *Abscissae*, all panels: time (minutes) after the addition of La^{3+}. *Ordinates*, *A*: unfiltered data, m_1 (millivolts), (Δ); m_2 (mV^2), (○); or m_3 (mV^3), (●). Log scales. Baseline $m_2 = (16 \pm 1) \times 10^{-3}\ mV^2$, baseline $m_3 = (0.22 \pm 1.1) \times 10^{-4}\ mV^3$. *B*: filtered data ($\tau = 3.1$ ms), m'_2 (millivolts squared), (○), or m'_3 (millivolts cubed), (●). Baseline $m'_2 = (0.80 \pm 0.16) \times 10^{-3}\ mV^2$, baseline $m'_3 = (0.35 \pm 0.18) \times 10^{-4}\ mV^3$. (*C* and *D*) Values of ξ and h calculated from m_1 and m_2 (unfiltered data), (Δ), m_3 and m_2 (unfiltered data), (●), or m'_3 and m'_2 (filtered data), (○). *Ordinates*: log scale for ξ (s^{-1}), linear scale for h (millivolts). The filled squares (■) indicate the average values of h (±SD) obtained by curve fitting 10 isolated mepps collected before La^{3+} was added and 10 others collected a few minutes after it was added. The crosses indicate frequencies measured by counting events displayed on a storage oscilloscope. This was feasible only when the frequency was $<200\ s^{-1}$. The bars indicate ±SD of the random errors estimated for filtered data as described in the text.

were obtained for m_3 (implying $h < 0$!) at the peak of secretion. In contrast, with filtered data m'_3 attained its peak near the moment of maximum depolarization (as expected), and in no case did it become negative. Figs. 5 *C* and *D* present the values of ξ and h determined from the moments shown in Figs. 5 *A* and *B*, using power spectra with the general shape illustrated in Fig. 2 *B*. The application of Campbell's theorem to m_1 and m_2 yields very small h and very large ξ over all but the first few minutes of the experiment. These seemingly unrealistic values occur because m_1 recovers more slowly than does m_2 (see also Katz and Miledi, 1972). The two sets of measurements of ξ and h based upon the variances and skews of either filtered or unfiltered data, respectively, agree well with one another except at the peak of secretion. During the late part of the experiment, when ξ had fallen to $<250\ s^{-1}$, it was determined directly by counting the number of mepps appearing in 20–30 intervals, each 200 ms in duration. The frequencies thus measured (× in Fig. 5 *C*) are quite consistent with the values of ξ computed from the variance and skew. At the peak of secretion, filtered and unfiltered data give very different results, but here the values derived from the analysis of unfiltered data are not valid: ξ would approach $10^6\ s^{-1}$, which is far beyond the theoretical upper limit for the measurement of mepp frequency, ξ_u. When ξ and h are obtained from filtered data, the maximum frequency is $5{,}200\ s^{-1}$, a value that does not exceed the theoretical limit of the method when applied to filtered data with these particular time constants (Theory). The random errors in the measurements of ξ and h were assessed as follows. (*a*) Individual values of ξ and h were obtained from m'_2 and m'_3 determined on successive single 10-s samples of filtered data; (*b*) these values were collected in groups of 12 (corresponding to 3-min periods) and the average and

standard deviation (SD) of each group were computed; (*c*) the SDs were divided by $3^{1/2}$ to give the expected SD for a triplet of estimates within that group. The error bars in the graphs indicate these SDs. Their normalized values ranged from 21% (peak of secretion) to <10% (after 50 min) for ξ, and from 11% (peak) to ~5% (after 50 min) for h.

In the early minutes of many of the experiments, and then again at the ends, ξ was such (~50 s^{-1}) that mepp parameters could be determined both by fluctuation analysis and by direct curve fitting of individual events. The agreement between the two sets of values is excellent for the time constants (least-squares slope equals 1.00, r = 0.987, N = 37), though less so for the h factor (unfiltered data: the slope equals 0.88, r = 0.695, N = 21; filtered

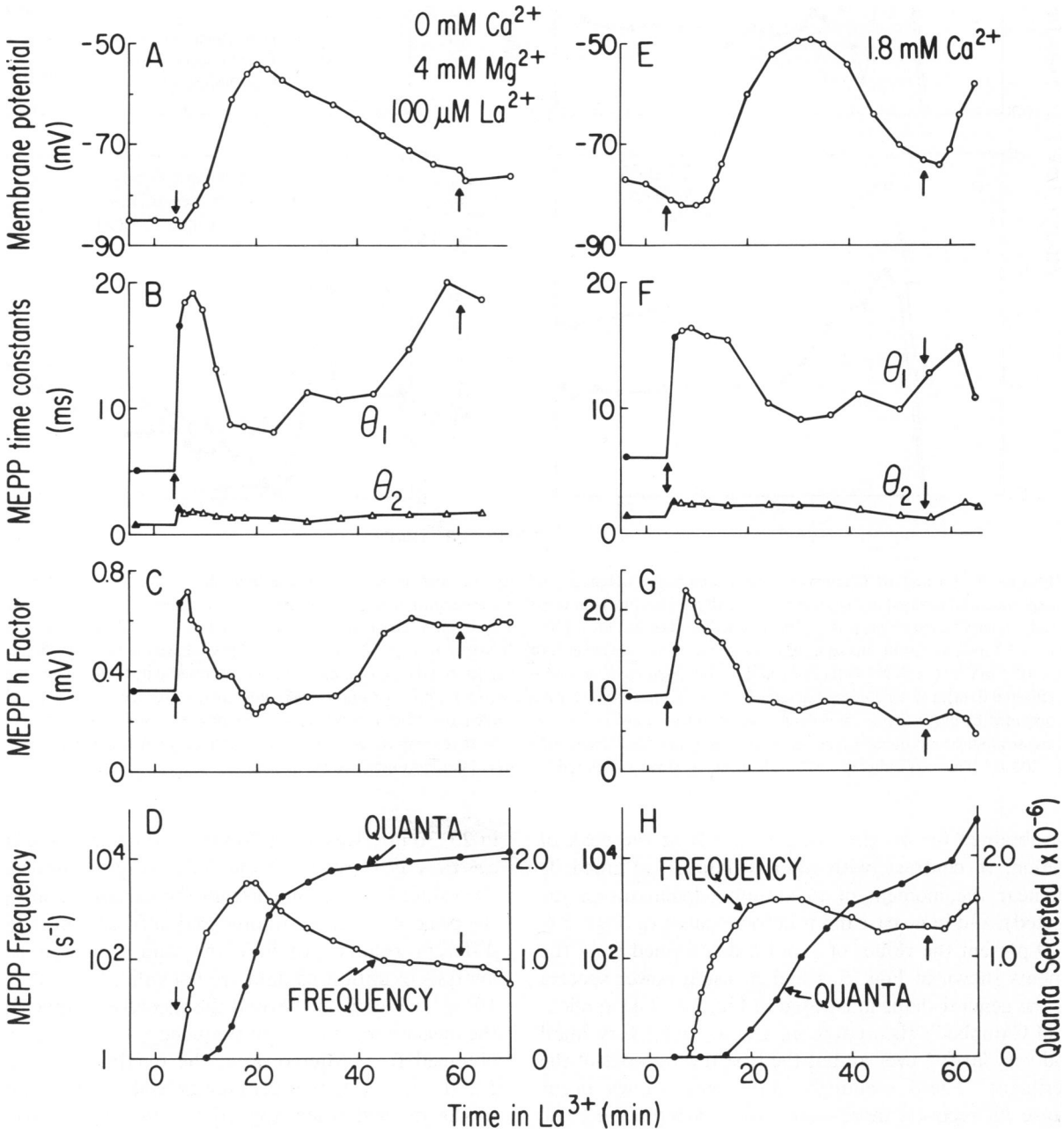

FIGURE 6 Time courses of the changes in membrane potential, θ_1, θ_2, h, mepp frequency, and number of quanta secreted at two different neuromuscular junctions following the application of 100 μM La^{3+} are shown. *Left* column of panels: junction bathed in modified Ringer's solution with 4 mM Mg^{2+} and no Ca^{2+}. *Right* column of panels: junction bathed in modified Ringer's solution with 4 mM Mg^{2+}. *Abscissae* all panels: time (minutes) after adding La^{3+}. Fresh La^{3+} solution was reapplied at the times indicated by the vertical arrows. The solid symbols plotted in *B*, *C*, *F*, and *G* are averages obtained by curve fitting ~10 individual mepps. In the experiment on the *right*, the final flush with La^{3+} evoked a second episode of rapid secretion.

data: the slope equals 0.83, $r = 0.645$, $N = 21$. The null hypothesis (no correlation) can be rejected for all comparisons at a $p < 0.01$ level.

Effect of La^{3+}

Fig. 6 illustrates the changes in membrane potential (*A*), mepp time constants (*B*), amplitude factor (*C*), and frequency (*D*), that occur when La^{3+} is applied in a Ca^{2+}-free solution with 4 mM Mg^{2+}. Initially, La^{3+} increased θ_1, θ_2, h, and ξ, but had little effect on V. As ξ rose to very large values, V, θ_1, and h decreased, passed through minima, and then slowly increased as ξ declined. The decline in ξ seemed to be hastened following renewal of the bathing solution. After its initial increase, θ_2 did not change much. About 2 million quanta were secreted during the 60-min measurement period, virtually all of them between 10 and 30 min after adding La^{3+}.

Similar changes occurred when La^{3+} was applied with 1.8 mM Ca^{2+} (Fig. 6 *E–H*), but several differences are apparent. (*a*) La^{3+} acted more slowly; (*b*) ξ rose to a maximum value only slightly above 1,000 s^{-1} and was sustained at a high level; (*c*) the membrane potential remained depolarized throughout the experiment; (*d*) after the usual initial increase, the h factor fell and remained small, relative to its peak, throughout the experiment; (*e*) when the bath was flushed, a new bout of secretion began (this was observed in only 2 of the 10 similar experiments with Ca^{2+}); and (*f*) the total number of quanta secreted was ~2.4 million, slightly more than were secreted in the absence of Ca^{2+}. These differences (except for the unusual second bout of secretion) were observed in five out of six experiments with junctions from paired muscles. In one of these experiments essentially no differences were observed between members of the pair (ξ_{peak} = 3,000 s^{-1}, ξ_{end} = 100 s^{-1} for both).

The major results from all our experiments are summarized in Table II. In general, ξ rose faster, reached higher maximum values, and fell to lower final levels when Ca^{2+} was absent than when present. The total number of quanta secreted in 1 h was similar in the two cases, but the temporal pattern of secretion was very different. The recoveries of V, θ_1, and h from their minima toward their initial values were more complete when Ca^{2+} was absent. Table II also lists the changes in V expected from the summation of mepps occurring at the peak of secretion and at the end of the experiments. The peak depolarizations, $E[\Delta V]$, were computed from Campbell's theorem using the values of ξ, h, θ_1, and θ_2 measured at the peak of secretion; they are several-fold smaller than those observed. If the initial values of h, θ_1, and θ_2 are used in the calculation, then $E[\Delta V]$ exceeds the measured ΔV by 10 mV (Ca^{2+} present) or by 30 mV (Ca^{2+} absent). These differences indicate either that the mepps do not sum linearly over the range of depolarization encountered in these experiments (Martin, 1955) or that only a small fraction of the depolarization is due to their summation. Either of these effects is sufficient to preclude using Campbell's theorem in its classic form, but neither contributes significantly to the power spectrum of the fluctuations (Fig. 2). Note that the mepps do sum linearly over the narrow range of potentials encompassed by the fluctuations, even though they sum nonlinearly over the much larger range of potentials of the depolarization from the resting level.

Table II also compares the fractional reductions in h, θ_1, and driving potential, V_d, that occurred at the peak depolarization. The driving potential was computed from the equation: $V_d = V - V_{eq}$, where V_{eq}, the equilibrium potential of the acetylcholine-gated endplate channels, was equated to -10 mV, a value in the middle of the range of experimental estimates (Takeuchi and Takeuchi, 1959; Lewis, 1979). The fractional reduction in h exceeds the fractional reductions in both V_d and θ_1 ($t > 2.8$, $p < 0.01$), but it is approximately equal to the product of the fractional reductions in V_d and θ_1. The significance of this correlation is discussed below.

Morphology

Fig. 7 illustrates the changes in nerve terminal ultrastructure that develop during 1 h of exposure at 22°C to a modified Ringer's solution with 100 μM La^{3+}, 1.8 mM Ca^{2+}, and 4 mM Mg^{2+}. Fig. 8 shows the modifications that occur in the absence of Ca^{2+}. Under both conditions, the number of synaptic vesicles declines markedly, and numerous intricately arranged swirls of membrane material appear in the axoplasm. Most of the swirls form closed loops and are composed of two closely apposed layers of membrane. In some sections the membrane swirls are continuous with the presynaptic axolemma, representing extensive invaginations of this structure that may be caused by the accumulation of vesicle membrane in it (see also Ceccarelli and Hurlbut, 1975).

Fig. 9 illustrates the results of the experiments with HRP: *a* and *c* are from a muscle soaked 0.5 h in a solution containing 100 μM La^{3+}, 4 mM Mg^{2+}, and 1.8 mM Ca^{2+}; *b* and *d* are from a muscle soaked 0.5 h in a Ca^{2+}-free solution with 100 μM La^{3+} and 4 mM Mg^{2+}. Electron-dense reaction product fills the vast extracellular space between muscle fibers, the extracellular space delimited by the pre- and post-synaptic membranes and the junctional folds, and the narrow extracellular space between the Schwann cell and the axolemma of the nerve terminal. Reaction product is also present in the *t*-tubules of the muscle fibers. Many synaptic vesicles are present in the axoplasm of both sets of nerve terminals, and some endocytotic vesicles containing reaction product are present. Reaction product is also found in the narrow spaces between the elaborate loops and swirls of membrane that resemble those seen in Figs. 7 and 8. This finding indicates that virtually all these loops and swirls are formed by extensive infoldings of the nerve terminal axolemma.

TABLE II
EFFECT OF La^{3+} ON MEPP PARAMETERS

Bathing solution (mM)		0.1 La^{3+} 1.8 Ca^{2+} 4 Mg^{2+}	0.1 La^{3+} 0 Ca^{2+} 4 Mg^{2+}	0.2 La^{3+} 0 Ca^{2+} 4 Mg^{2+}	1.0 La^{3+} 1.8 Ca^{2+} 0 Mg^{2+}
Temperature (°C)		22–25	22–25	16–17	2–3
Number of junctions		6	5	2	1
Time-to-peak (min)		13 ± 7	9 ± 6	5 ± 1	17
θ_1 (ms)	control	5.2 ± 0.7	6.0 ± 2.8	5.9 ± 0.4	27
	initial	13.3 ± 5.2*	13.3 ± 3.7	10.0 ± 1.7	43
	peak	7.7 ± 3.6	7.5 ± 1.2	7.3 ± 1.0	25
	final	9.3 ± 4.0	12.2 ± 3.4	10.4 ± 2.5	28
θ_2 (ms)	control	1.0 ± 0.2	1.0 ± 0.3	1.1 ± 0.3	5.4
	initial	1.5 ± 0.6*	1.8 ± 0.5	1.6 ± 0.2	5.4
	peak	1.4 ± 0.5	1.6 ± 0.3	1.5 ± 0.1	4.4
	final	1.3 ± 0.6	1.4 ± 0.2	1.5 ± 0.3	5.8
h (mV)	control	0.72 ± 0.13	0.60 ± 0.19	0.53 ±0.00	0.61
	initial	1.42 ± 0.66*	1.06 ± 0.28	1.10 ± 0.4	0.67
	peak	0.51 ± 0.21	0.36 ± 0.14	0.38 ± 0.06	0.17
	final	0.65 ± 0.23	0.78 ± 0.27	0.97 ± 0.42	0.35
ξ (s^{-1})	peak × 10^{-3}	2.2 ± 1.0	4.5 ± 2.3	2.0 ± 0.5	0.38
	final	500 ± 670	50 ± 60	15 ± 5	12
Quanta secreted × 10^{-6} (1 h)		2.5 ± 0.8	2.2 ± 0.9	0.8	0.42
V (mV)	initial	−91 ± 6	−89 ± 6	−61 ± 1	−63
	peak	−64 ± 10	−62 ± 8	−47 ± 2	−55
	final	−81 ± 15	−86 ± 7	−58 ± 1	−63
ΔV‡ (mV)	peak	27 ± 6	26 ± 8	15 ± 1	8
	final	10 ± 9	3 ± 2	4 ± 2	0
$E[\Delta V]$§ (mV)	peak	6.2 ± 3.8	8.8 ± 5.1	4.2 ± 1.2	1.3
	final	2.7 ± 3.8	0.2 ± 0.1	0.1	0.1
$V_d\left[\frac{\text{peak}}{\text{initial}}\right]$‖		0.68 ± 0.12	0.65 ± 0.11	0.71 ± 0.01	0.85
$\theta_1\left[\frac{\text{peak}}{\text{initial}}\right]$		0.65 ± 0.11*	0.59 ± 0.14	0.72 ± 0.04	0.58
$h\left[\frac{\text{peak}}{\text{initial}}\right]$		0.39 ± 0.10*	0.34 ± 0.14	0.36 ± 0.08	0.25

Controls equals individual fit before La^{3+}; initial, peak, and final equal the values from fluctuation analysis during initial, peak, and final stages of La^{3+}-induced secretion.

*Reliable initial values were obtained in only four of the six experiments.

‡Change of V from initial value.

§Expected depolarization = $\xi h(\theta_1 - \theta_2)$.

‖ $V_d = (V - V_{eq})$ (see text).

FIGURE 7 Changes in the ultrastructure of frog neuromuscular junctions treated for 1 h with a modified Ringer's solution containing 100 μM La^{3+}, 1.8 mM Ca^{2+}, and 4 mM Mg^{2+}. Longitudinal sections. (*a*) Control muscle soaked for 1 h in solution without La^{3+}. (*A*) Axoplasm of nerve terminal; (*S*) nucleus of Schwann cell; (*M*) myoplasm. The axoplasm contains mitochondria, neurofilaments, and numerous synaptic vesicles. Note that vesicles are not distributed uniformly within the axoplasm of a given terminal, and that large differences in vesicle concentration occur among different terminals (compare with Fig. 8 *a*). *b* and *c* terminals from two different muscles soaked for 1 h in a solution with 100 μM La^{3+}. The number of synaptic vesicles is clearly reduced, and the axoplasm contains numerous loops and swirls of membrane material arranged as closely apposed pairs, many of which are continuous with the presynaptic membrane (arrow). Some coated vesicles are also present. Large aggregates (arrowhead), or punctate deposits, of La^{3+} are present in the synaptic cleft and junctional folds. (*a*) ×18,700; (*b*) ×24,700; (*c*) ×20,500.

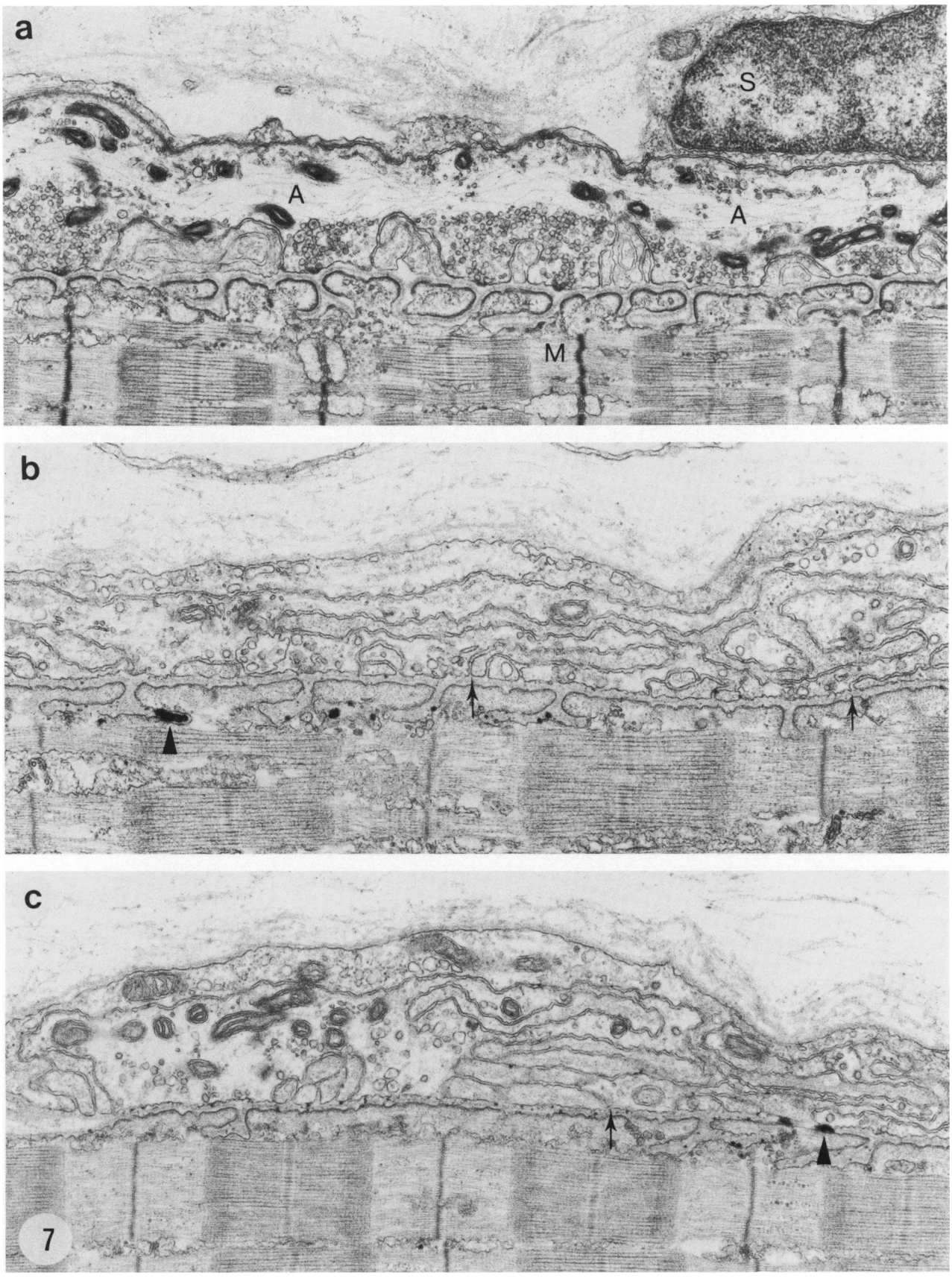
a
S
A
A
M
b
c
7

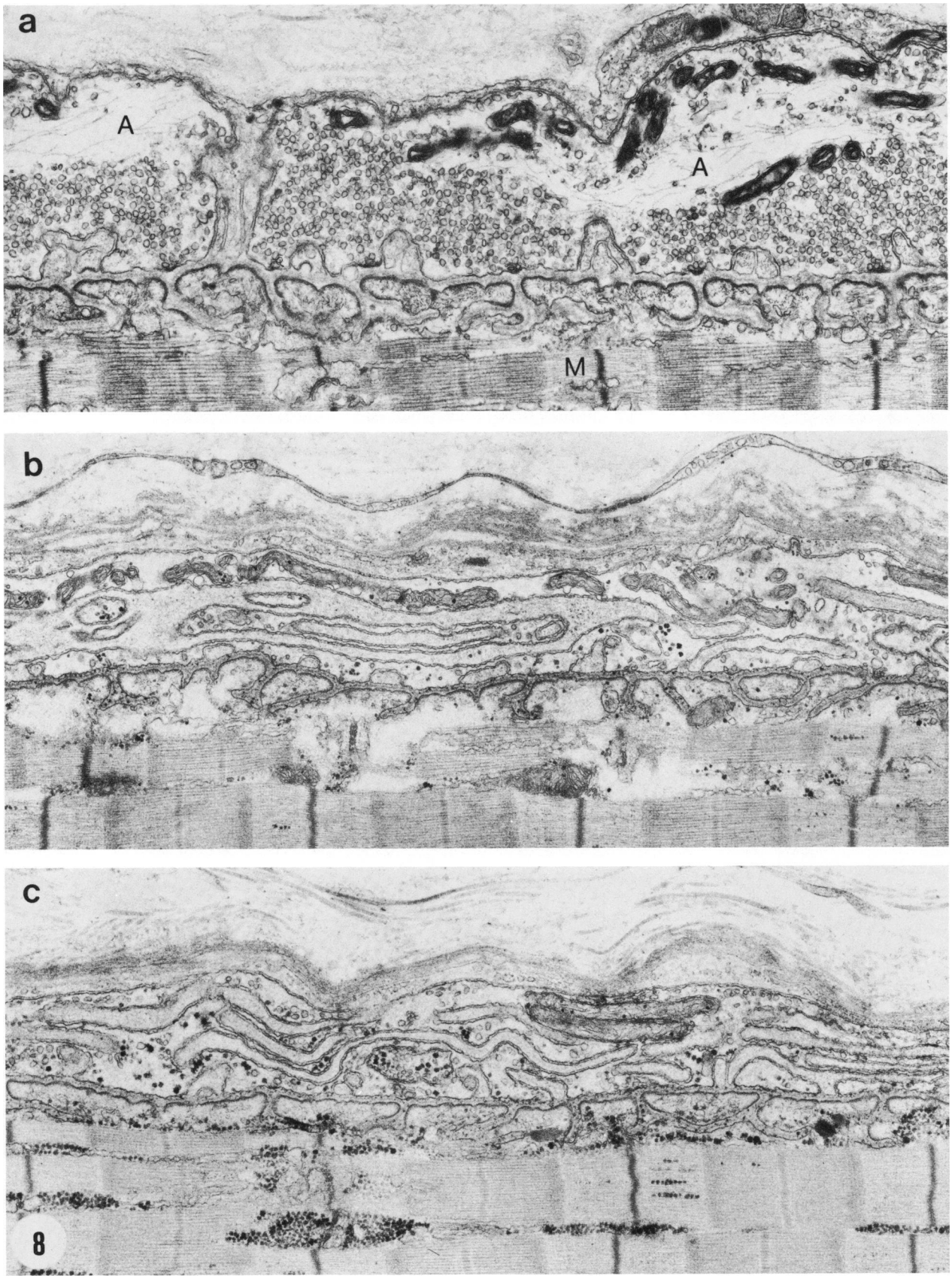
a
A
A
M
b
c
8

These infoldings were previously observed in cross-sectioned terminals but were interpreted as isolated cysternae not connected with the extracellular space (Heuser and Miledi, 1971). Control terminals that have been exposed to HRP and myoglobin but not to La^{3+} do not show infoldings of the axolemma, and the extracellular tracers do not enter the axoplasm or its synaptic vesicles, in agreement with previous results (Ceccarelli et al., 1972, 1973; Ceccarelli and Hurlbut, 1975).

Table III summarizes the results of morphometric measurements on sections of terminals at rest or after exposure to La^{3+} for 1 h. The average density of synaptic vesicles declined to 28% of the control value when Ca^{2+} was present and to 13% when Ca^{2+} was absent. These changes are statistically significant. The number of large vesicular structures increased slightly in the terminals treated with La^{3+} and Ca^{2+}. The average density of synaptic vesicles measured in our control sections is 51 ± 24 vesicles/μm^2 of axoplasm. Since the thickness of the sections is ~40 nm (silver-gray color)(Weibel and Paumgartner, 1978), the apparent concentration of synaptic vesicles is 1,200 ± 600/μm^3. This figure is an overestimate since the count on each section includes vesicles whose centers lie outside the section, and, therefore, it should be reduced by the factor $(1 + d/L)$ where d is the vesicle diameter (~40 nm) and L the section thickness. Thus, the corrected vesicle concentration is ~600 ± 300 vesicles/μm^3 (~60% of that estimated previously by Birks et al. [1960] for terminals in frog sartorius muscle). The average length of a terminal in frog cutaneous pectoris muscle is 600 ± 200 μm (Letinsky et al., 1976; Valtorta et al., 1984) and the diameter is 1.3 ± 0.35 μm. The latter measurements were made on muscles fixed and processed with the same procedures used here. When these figures are combined with our vesicle counts, a value of $(4.8 \pm 3.4) \times 10^5$ is obtained for the number of vesicles in unstimulated terminals.

DISCUSSION

The power spectrum, variance, and skew of the signal recorded at vigorously secreting neuromuscular junctions can be used to measure mepp amplitude, h, waveform, $F(t)$, and frequency of occurrence, ξ, over a wide range of conditions. Computer simulations of ideal situations show that the moments depend upon h, ξ, and $F(t)$ in the manner expected from theory, and that valid estimates of h and ξ are obtained for frequencies ranging from 10 to ~10^4 s^{-1}. Experimentally, we find that single mepps can be represented as the difference between two exponentials and that the power spectra obtained at La^{3+}-stimulated junctions are well fit, even at times of most vigorous secretion, by the spectrum corresponding to such unitary events. This close correspondence indicates that the mepps occur independently and at a frequency that is reasonably stationary over the spectral analysis sampling period (4 s). On the other hand, changes in $\xi(t)$ that develop over the 10-s sampling period employed for the measurement of the moments might not be revealed in power spectra like ours (low-frequency limit of 0.25 Hz) but would introduce bias errors into the estimates of ξ and h. However, both the theoretical analysis (Appendix) and the results of computer simulation (Results) show that these errors are almost completely eliminated when the data are filtered.

Our assumption that h is the same for all mepps occurring within a 10-s interval introduces a bias error into our estimates of h and ξ. For h variable, the form of the semi-invariants is $\lambda_n = \bar{h}^n I_n$ (Rice, 1944), where the bar denotes the average over the population, and the appropriate equations for m_2 and m_3 are: $m_2 = \xi(\bar{h})^2 (1 + \Delta^2) I_2$ and $m_3 = \xi(\bar{h})^3 (1 + 3\Delta^2 + \gamma^3) I_3$, where $\bar{h}$ = mean h, Δ = coefficient of variation of h, and γ^3 = (skew of h)/$(\bar{h})^3$. Since the amplitude distribution of mepps recorded at a single junction is approximately Gaussian (del Castillo and Katz, 1954), γ will be small, and the equations for $\bar{h}$ and ξ become

$$\bar{h} = \frac{m_3 I_2 (1 + \Delta^2)}{m_2 I_3 (1 + 3\Delta^2)} = \bar{h}_a \frac{(1 + \Delta^2)}{(1 + 3\Delta^2)}$$

$$\xi = \frac{(m_2)^3 (I_3)^2 (1 + 3\Delta^2)^2}{(m_3)^2 (I_2)^3 (1 + \Delta^2)^3} = \xi_a \frac{(1 + 3\Delta^2)^2}{(1 + \Delta^2)^3},$$

where $\bar{h}_a$ and ξ_a are the apparent h and ξ as presented in our results. The coefficients of variation of h from our data are ~30%, (Table I), a value similar to that observed by others (del Castillo and Katz, 1954). Thus, by assuming h to be uniform, we may have overestimated h by ~18% and underestimated ξ by ~27%. If Δ increases at La^{3+}-stimulated junctions, as the observations of Kriebel and Florey (1983) indicate, then the errors will be greater than estimated here. On the other hand, we found that whenever h and ξ could be determined both from measurements on individual mepps and from fluctuation analysis, the differences between the two sets of values were smaller than this estimated error (see Results and Fig. 5 *C*). A smaller error would be expected if h and I_n were inversely correlated for individual mepps, and the data in Table I suggest this may the case since the coefficients of variation of the measured

FIGURE 8 Changes in the ultrastructure of frog neuromuscular junctions treated for 1 h with a modified Ringer's solution containing 100 μM La^{3+}, 4 mM Mg^{2+}, and no added Ca^{2+}. Longitudinal sections. (*a*) Control terminal soaked for 1 h in the Ca^{2+}-free solution without La^{3+}. Although more synaptic vesicles are present in this section, the ultrastructure of the terminal is similar to that of Fig. 7 *a*. (*A*) Axoplasm; (*M*) myoplasm. *b* and *c* terminals from two different muscles soaked for 1 h in the Ca^{2+}-free solution with 100 μM La^{3+}. These terminals resemble those shown in Fig. 7 *b* and *c*: The number of synaptic vesicles is much reduced, and the axoplasm contains numerous elaborate infoldings of the axolemma. Fine deposits of La^{3+} are present within the infoldings and in the synaptic cleft. (*a*) ×20,500; (*b*) ×18,500; (*c*) ×20,000.

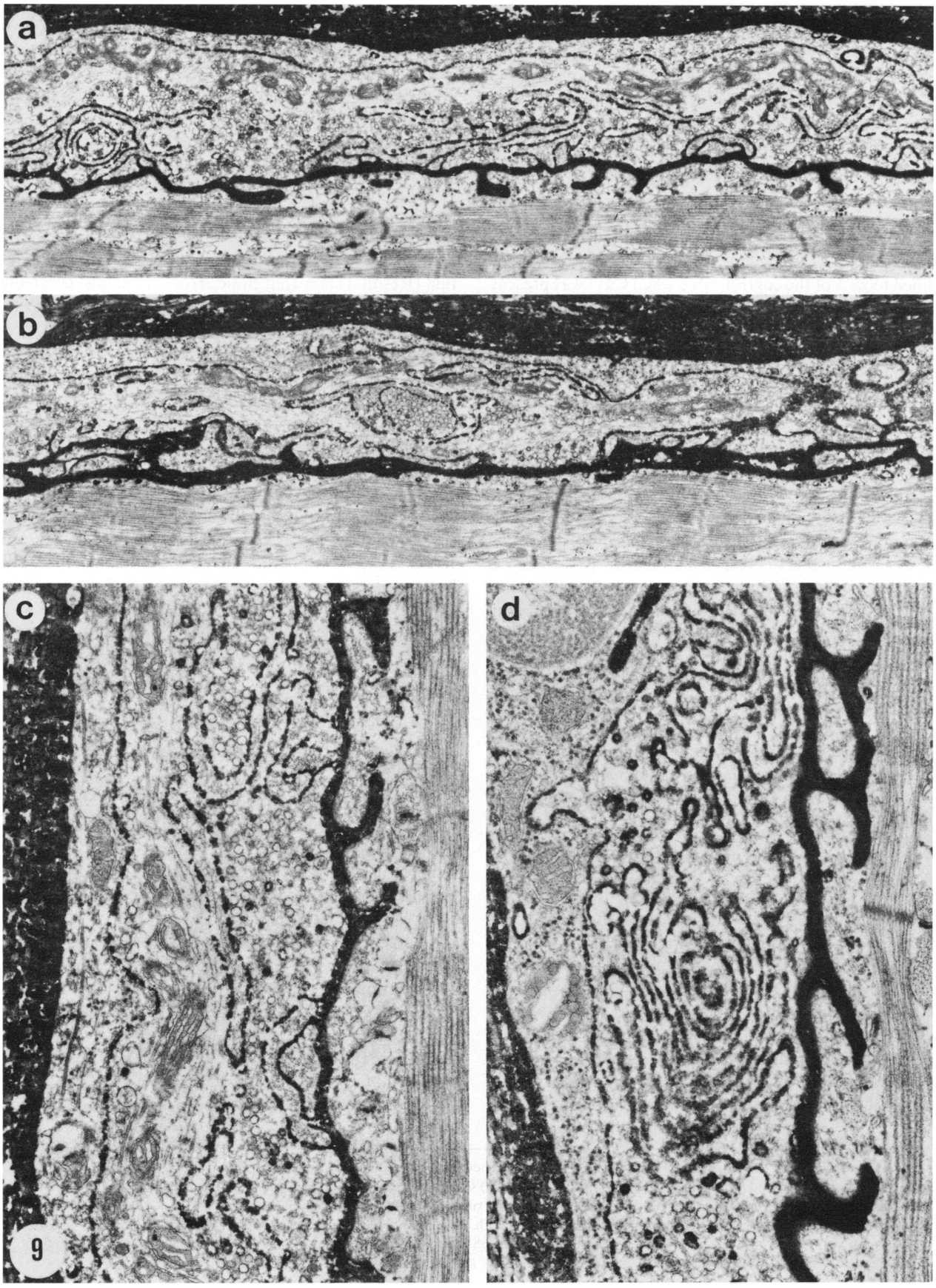
a
b
c
d
g

TABLE III
EFFECT OF La^{3+} AND Ca^{2+} ON NERVE TERMINAL ULTRASTRUCTURE

	Total quantity measured		
	Control (15)	La^{3+} + Ca^{2+} (16)	La^{3+} no Ca^{2+} (17)
Axoplasm area (μm^2)	240	110	113
Axolemma length (μm)	381	273	313
Infoldings length (μm)	4	249	282
LVS* (number)	216	292	107
SV‡ (number)	12.2×10^3	1.5×10^3	0.7×10^3
Normalized per μm^2 of axoplasm			
Axolemma length ($\mu m/\mu m^2$)	1.63 ±0.30	2.56 ±0.26	2.91 ±0.57
Infoldings length§ ($\mu m/\mu m^2$)	0.02 ±0.07	2.17 ±1.83	2.61 ±2.25
LVS perimeter ($\mu m/\mu m^2$)	0.31 ±0.16	0.85 ±0.34	0.33 ±0.29
SV (number/μm^2)	51 ±24	14‖ ±4.5	6.8‖ ±2.4

Numbers in parentheses are the number of micrographs examined.
*LVS = Large vesicular structures.
‡SV = Synaptic vesicle.
§The length of membrane is about twice the length of the infoldings.
‖ Values significantly different from control and from each other ($t = 5.6$, $p < 0.001$).

integrals, J_n, are smaller than the sum of the coefficients of variation of h and I_n. Such a correlation would arise, for example, from the cable properties of the junction.

Variations in the time course of individual mepps might also affect the accuracy of our estimates of ξ and h. These variations occur in part because frog motor nerve terminals are long and the mepps are distorted by the cable properties of the endplate. Such distortions also imply that the mepp cannot be described precisely as the sum of two exponentials. However, as pointed out above, the successful application of Campbell's theorem does not require that every single event be exactly reproduced by $F(t)$: it is sufficient that a single waveform represents the average integrals, J_n, over the population, and both our observations on individual mepps and the good fit of power spectra show this to be true. A striking demonstration that $F(t)$ need only reproduce the average behavior of the population of elementary events and need not reproduce precisely the individual events is provided by the analysis of channel noise. The real elementary event in this case is a square pulse of fixed amplitude and random duration with average value τ. A randomly occurring population of these events is equivalent to a population of exponential events with the same amplitude and fixed time constant τ (see e.g., Katz and Miledi, 1972).

The procedure described here for measuring ξ and h at rapidly secreting junctions has been developed to study the temporal pattern of quantal secretion and thereby to determine the kinetics of quantal turnover and vesicle recycling. Three quantities are required to determine the extent of quantal turnover during a period of secretion: the total number of quanta secreted, the number initially present within the terminal, and the number remaining at the end. The integral over time of the rate of quantal secretion yields a figure of $\sim 2 \times 10^6$ for the number of quanta released during our experiments. Previous estimates of the initial store of quanta in nerve terminals in frog cutaneous pectoris muscle vary from 2.5×10^5 to 6×10^5 (Ceccarelli et al., 1973; Ceccarelli and Hurlbut, 1975). Our present estimate of the number of synaptic vesicles in control terminals spans this range. If a quantum is secreted by the fusion of a vesicle with the axolemma, then our results imply that vesicle population must have turned over several times during the hour of secretion in La^{3+}. Further support for this conclusion is the observation that the endocytosis of HRP by nerve terminals is accelerated under these conditions.

An upper limit to the number of quanta in a resting nerve terminal would be given by using the present technique to determine the total number of quanta secreted following application of black widow spider venom (BWSV) in a Ca^{2+}-free solution. Quantal secretion ceases within 1 h under such conditions, and the terminals are totally depleted of vesicles (Longenecker et al., 1970; Clark et al., 1972; Hurlbut and Ceccarelli, 1979), apparently because BWSV interferes with recycling (Ceccarelli and Hurlbut, 1980*b*). We have studied BWSV-stimulated terminals, but, unfortunately, the power spectra do not approach the theoretical low-frequency slope of zero in

FIGURE 9 Effect of Ca^{2+} on the distribution of HRP in terminals treated for 0.5 h with modified Ringer's solution containing 100 μM La^{3+}. Longitudinal sections. (*a* and *c*) two different sections of a terminal from a muscle treated with a solution containing 1.8 mM Ca^{2+} and 4 mM Mg^{2+}. Reaction product is seen in the extracellular spaces, including the synaptic cleft, the junctional folds, the space between Schwann cell and nerve terminal axolemma, and the spaces delimited by the elaborate infoldings of the axolemma. Many synaptic vesicles are still present after this relatively short exposure to La^{3+}, and some are loaded with reaction product. (*b* and *d*) Sections from two different terminals of a muscle treated with La^{3+} in a Ca^{2+}-free solution. The distribution of reaction product is similar to that seen in *a* and *c*, but fewer synaptic vesicles are present. The smaller number of vesicles seen when Ca^{2+} is absent is consistent with the more rapid onset and more intense secretion that occur in this condition (Fig. 6 and Table II). (*a*) ×14,500; (*b*) ×15,300; (*c*) ×28,000; (*d*) ×32,800.

log-log plots, as in Fig. 2, rather they continue to rise down to the lowest frequencies measured. Until the origin of this low frequency behavior of the power spectrum can be accounted for, it would be unwise to try to calculate ξ from these data.

At the peak of secretion h fell by 60–70% and remained low if high rates of secretion were sustained (Table II). Decreases in h can be caused by many factors: diminution of quantal size, i.e., the number of ACh molecules contained in a quantum, reduction in the potential that drives ions through the ACh-gated channels in the endplate, desensitization of the junctional receptors to ACh, and a rise of membrane conductance of the muscle fiber. It is important to determine how much, if any, of the observed fall in h is due to a decrease in quantal size since, according to the vesicle hypothesis, its changes should reflect the rate at which recycled vesicles are restocked with transmitter (Knight, 1973). The fall in h that we observed was approximately equal to the product of the reduction in driving potential times the reduction in θ_1 (Table II). Since θ_1 reflects the time constant of the endplate membrane (Fatt and Katz, 1951), the fall in θ_1 suggests that the resistance of the endplate was reduced at the peak of secretion. Therefore, the reduction in h may have been due entirely to changes in the electrical properties of the endplate while quantal size remained constant even at rates of secretion near 5,000 s^{-1}. However, the prediction of how h is affected by membrane resistance, R_m, is crucially dependent upon the equivalent circuit used to represent the endplate membrane. A simple equivalent circuit, which ignores membrane capacitance, predicts that h is strongly dependent upon R_m and accounts for nonlinear summation (Martin, 1955). If a simple membrane capacitance, C_m, is added to the equivalent circuit, then h becomes almost independent of R_m (Hubbard et al., 1969). Since the true equivalent circuit of a muscle fiber is more complicated than a simple R_mC_m (Falk and Fatt, 1964), it is not straightforward to account for the large change in h, a priori. Measurements under voltage clamp and during iontophoretic application of ACh should be helpful.

APPENDIX

Effect of Nonstationarity on the Estimates of h and ξ

Eq. 1 (Theory) is derived under the assumptions that ξ, h, and $F(t)$ are fixed and that the probability of occurrence of a single event is governed by Poisson statistics (Rice, 1944). In our experiments ξ, h, and $F(t)$ change during the period of secretion, and we need to evaluate the errors introduced into the estimates of these parameters by the nonstationary conditions. The assumption of stationarity is important not only to the derivation of Eq. 1 but also to the way data are collected and analyzed. Strictly speaking, the analysis of random data requires averaging over ensembles of records, and time averaging over an individual record can be substituted only when the random process is ergodic (Bendat and Piersol, 1971). A process must be stationary to be ergodic (Bendat and Piersol, 1971). Thus, in principle, if a random process is not stationary, then its characteristic moments should not be computed by time averaging over individual records, as we must do in our experiments. We give below a somewhat heuristic analysis that indicates that, when the elementary event has an integral equal to zero ($I_1 = 0$, i.e., filtered data), the expected values of the moments determined by time averaging individual records are equal to the expected values of the time averages of the corresponding moments determined from ensembles of records, even when the process is not stationary, provided that the probability of occurrence of the events is approximately constant over the duration of one elementary event. When the two sets of moments can be equated, it is easy to estimate the bias errors introduced by nonstationarity, and the analysis shows that these errors are small.

Rice (1944) has treated the case where ξ changes with time. He considers an ensemble of records each of duration T. The (ensemble) average number of events that occur during the interval T is $\bar{K}$. The expected number of events occurring between t and $t + dt$ within the interval T is $\bar{K}p(t)dt$, where $\int_0^T p(t)dt = 1$. Thus $\bar{K}p(t)$ can be interpreted as an instantaneous frequency. The expected values of the mean, variance, and skew of the fluctuations in potential determined from the ensemble of such records are functions of time and are given by the equation

$$M_n(t) = \bar{K}h^n \int_0^T p(\tau)\,[F(t-\tau)]^n d\tau.$$

If $p(t)$ does not change appreciably during the time course of a single event and if T is much greater than the duration of a single event, then the expected values of the moments become

$$M_n(t) \simeq \bar{K}p(t)h^nI_n = \xi(t)h^nI_n, \qquad \text{(A1)}$$

where $\xi(t) = \bar{K}p(t)$ is the instantaneous frequency. Their averages over the interval T are given by $\langle M_n \rangle = h^nI_n\langle \xi \rangle$.

When the $\langle M_n \rangle$ are determined empirically from an ensemble of N records

$$M_1(t) = \frac{1}{N}\sum_{r=1}^{N} V_r(t),$$

where V_r is the potential at time t in record r, and the time averaged variance and skew are

$$\langle M_n \rangle = \frac{1}{N}\sum_{r=1}^{N}\frac{1}{T}\int_0^T [V_r(t) - M_1(t)]^n dt \quad \{n = 2, 3\}, \qquad \text{(A2)}$$

where the order of integration and summation has been reversed.

In our experiments we do not compute averages over ensembles of records. We collect sequential digitized samples of the voltage during a single sampling period of duration T. The interval between digitized samples is short compared with the duration of the mepp so that the moments we compute can be represented as

$$m_n = \frac{1}{T}\int_0^T [V(t) - m_1]^n dt \quad \{n = 2, 3\}, \qquad \text{(A3)}$$

where $m_1 = \langle V(t) \rangle$. If Eq. A3 is compared with Eq. A2, we see that the moments, m_n, differ in two major respects from the moments, $\langle M_n \rangle$. First, the latter moments approach the expected values more closely since they are averages over N records. Second, and more important, the two values from which the fluctuations are computed, m_1 and $M_1(t)$, differ fundamentally in that m_1 is constant while $M_1(t)$ changes with time. Thus, for higher moments, $m_n \neq \langle M_n \rangle$, i.e., the moments determined by time averaging single records are not equal to the time averages of the moments determined from ensembles of records. However, when $I_1 = 0$ (i.e., filtered data), then both $M_1(t)$ and m_1 are almost zero, and the moments $\langle M_n \rangle$ and m_n become almost equal, except that the former have smaller random errors since they are computed from a larger sample of data. The size of the random errors in the values of the moments determined from a single record depends upon the number of events that

occurred during the record. If $\xi = 10\ s^{-1}$, then 100 events are expected to occur during a 10-s sampling period, and the random fluctuations in this number are expected to be 10%. This value of ξ should represent a reasonable lower frequency limit for the application of our procedure.

If both h and ξ change with time (and are uncorrelated), we extend (heuristically) the above results to get

$$m_n = I_n \frac{1}{T}\int_0^T \xi(t)h^n(t)dt = I_n \langle \xi h^n \rangle \quad \{n = 2, 3\}.$$

The estimated values for h and ξ are

$$\bar{h} = \frac{m_3 I_2}{m_2 I_3} = \frac{\langle \xi h^3 \rangle}{\langle \xi h^2 \rangle}$$

$$\bar{\xi} = \frac{M_2^3 I_3^2}{m_3^2 I_2^2} = \frac{\langle \xi h^2 \rangle^3}{\langle \xi h^3 \rangle^2}.$$

Consider the particular case where ξ and h change exponentially with time: $\xi = \xi_c e^{a(t-T/2)}$ and $h = h_c e^{b(t-T/2)}$. In our most extreme experiment ξ increased from ~1 to ~7,000 s^{-1}, and h decreased from ~1 to ~0.3 mV during the second and third minutes after the application of La^{3+}. In this case $a \simeq 0.1\ s^{-1}$ and $b \simeq -0.01\ s^{-1}$. Our sampling period is 10 s so we have $\tilde{h} = 0.99h_c = 0.99\bar{h}$ and $\tilde{\xi} = 1.04\xi_c = \bar{\xi}$, where $\bar{\xi}$ and $\bar{h}$ are the average values of ξ and h over the interval T. Thus even in this most extreme case the nonstationarity of the data introduces errors of only a few percent into the estimates of ξ and h determined over a single sampling interval. These small bias errors are much less than the random errors.

To reduce the size of the random errors in our experimental data, we averaged the moments computed from three successive 10-s periods of data collection (separated from one another by 5-s periods of computation) and used the resulting mean values to compute single values of ξ and h. If we apply the above analysis to the entire 40-s interval over which these data were collected, we obtain: $\tilde{\xi} = 1.08\bar{\xi}$, $\tilde{h} = 0.89\bar{h}$. Although these bias errors are larger than those for a single sampling period, they still are smaller than the random errors obtained from simulated data. These results are consistent with the results of the simulations.

We thank Professor Bruce W. Knight, Jr. for his encouragement and cogent advice and for helping us to evaluate the effects of nonstationarity. We are indebted to Dr. Daniel Tranchina for alerting us to the potential problems associated with nonstationarity, for discussing the difficulties with us, and for reading and criticizing several drafts of the Appendix. We thank Numa Iezzi for his patient help with the electron microscopy, and Paolo Tinelli and Franco Crippa, who prepared Figs. 7, 8, and 9.

Supported by the Veterans Administration (J. R. Segal), a Muscular Dystrophy Association grant (B. Ceccarelli) and a Muscular Dystrophy Association grant and a U.S. Public Health Service grant NS18354 (W. P. Hurlbut).

Received for publication 16 December 1983 and in final form 15 August 1984.

REFERENCES

Anderson, C. R., and C. F. Stevens. 1973. Voltage clamp analysis of acetylcholine produced end-plate current fluctuations at frog neuromuscular junction. *J. Physiol.* (*Lond.*). 235:655–691.

Bendat, J. S., and A. G. Piersol. 1971. Random Data: Analysis and Measurement. John Wiley and Sons, Inc., New York.

Birks, R., H. E. Huxley, and B. Katz. 1960. The fine structure of the neuromuscular junction of the frog. *J. Physiol.* (*Lond.*). 150:134–144.

Campbell, N. 1909. The study of discontinuous phenomena. *Proc. Cambridge. Phil. Soc.* 15:117–136.

Ceccarelli, B., F. Grohovaz, and W. P. Hurlbut. 1979*a*. Freeze-fracture studies of frog neuromuscular junctions during intense release of neurotransmitter. I. Effect of black widow spider venom and Ca^{2+}-free solutions on the structure of the active zone. *J. Cell Biol.* 81:163–177.

Ceccarelli, B., F. Grohovaz, and W. P. Hurlbut. 1979*b*. Freeze-fracture studies of frog neuromuscular junctions during intense release of neurotransmitter. II. Effects of electrical stimulation and high potassium. *J. Cell Biol.* 81:178–192.

Ceccarelli, B., and W. P. Hurlbut. 1975. The effects of prolonged repetitive stimulation in hemicholinium on the frog neuromuscular junction. *J. Physiol.* (*Lond.*). 247:163–188.

Ceccarelli, B., and W. P. Hurlbut. 1980*a*. Ca^{2+}-dependent recycling of synaptic vesicles at the frog neuromuscular junction. *J. Cell Biol.* 87:297–303.

Ceccarelli, B., and W. P. Hurlbut. 1980*b*. Vesicle hypothesis of the release of quanta of acetylcholine. *Physiol. Rev.* 60:396–441.

Ceccarelli, B., W. P. Hurlbut, and A. Mauro. 1972. Depletion of vesicles from frog neuromuscular junctions by prolonged tetanic stimulation. *J. Cell Biol.* 54:30–38.

Ceccarelli, B., W. P. Hurlbut, and A. Mauro. 1973. Turnover of transmitter and synaptic vesicles at the frog neuromuscular junction. *J. Cell Biol.* 57:499–524.

Clark, A. W., W. P. Hurlbut, and A. Mauro. 1972. Changes in the fine structure of the neuromuscular junction of the frog caused by black widow spider venom. *J. Cell Biol.* 52:1–14.

De Bassio, W. A., R. M. Schnitzler, and R. L. Parsons. 1971. Influence of lanthanum on transmitter release at the neuromuscular junction. *J. Neurobiol.* 2:263–278.

del Castillo, J., and B. Katz. 1954. Quantal components of the end-plate potential. *J. Physiol.* (*Lond.*). 124:560–573.

del Castillo, J., and B. Katz. 1956. Biophysical aspects of neuro-muscular transmission. *Prog. Biophys. Biophys. Chem.* 6:121–170.

Dodge, F., B. W. Knight, and J. Toyoda. 1968. Voltage noise in *Limulus* visual cells. *Science* (*Wash. DC*). 160:88–90.

Falk, G., and P. Fatt. 1964. Linear electrical properties of striated muscle fibers observed with intracellular electrodes. *Proc. Roy. Soc. Lond. Ser. B.* 160:69–123.

Fatt, P., and B. Katz. 1951. An analysis of the end-plate potential recorded with an intracellular electrode. *J. Physiol.* (*Lond.*). 115:320–370.

Fatt, P., and B. Katz. 1952. Spontaneous subthreshold activity at motor nerve endings. *J. Physiol.* (*Lond.*). 117:109–128.

Heuser, J., and R. Miledi. 1971. Effect of lanthanum ions on function and structure of frog neuromuscular junction. *Proc. Roy. Soc. Lond. Ser. B.* 179:247–260.

Heuser, J. E., and T. S. Reese. 1973. Evidence for recycling of synaptic vesicle membrane during transmitter release at the frog neuromuscular junction. *J. Cell Biol.* 57:315–344.

Heuser, J. E., T. S. Reese, M. J. Dennis, Y. Jan, L. Jan, and L. Evans. 1979. Synaptic vesicle exocytosis captured by quick freezing and correlated with quantal transmitter release. *J. Cell Biol.* 81:275–300.

Holtzman, E., A. R. Freeman, and L. A. Kashner. 1971. Stimulation dependent alterations in peroxidase uptake at lobster neuromuscular junctions. *Science* (*Wash. DC*). 173:733–736.

Hubbard, J. I., R. Llinás and D. M. J. Quastel. 1969. Electrophysiological Analysis of Synaptic Transmission. E. J. Arnold & Son Ltd., London.

Hurlbut, W. P., and B. Ceccarelli. 1979. The use of black widow spider venom to study the release of neurotransmitters. *Adv. Cytopharmacol.* 3:87–115.

Katz, B., and R. Miledi. 1972. The statistical nature of the acetylcholine potential and its molecular components. *J. Physiol.* (*Lond.*). 224:665–699.

Katz, B., and R. Miledi. 1977. Transmitter leakage from motor nerve endings. *Proc. Roy. Soc. Lond. Ser. B.* 196:59–72.

Knight, B. W. 1973. A stochastic problem in visual neurophysiology. *In* American Mathematical Society Symposium on Stochastic Differential Equations. J. Keller and H. J. McKean, editors. American Mathematical Society, Providence, RI. 1–19.

Kriebel, M. E., and E. Florey. 1983. Effect of lanthanum ions on the

amplitude distributions of miniature endplate potentials and on synaptic vesicles in frog neuromuscular junctions. *Neuroscience.* 9:535–547.

Lambert, D.H., and R.L. Parsons. 1970. Influence of polyvalent cations on the activation of muscle end plate receptors. *J. Gen. Physiol.* 56:309–321.

Letinsky, M. S., K. H. Fishbeck, and U. J. McMahan. 1976. Precision of reinnervation of original post-synaptic sites in frog muscle after a nerve crush. *J. Neurocytol.* 5:691–718.

Lewis, C. A. 1979. Ion concentration dependence of the reversal potential and the single channel conductance of ion channels at the frog neuromuscular junction. *J. Physiol. (Lond.).* 286:417–445.

Longenecker, H. B., W. P. Hurlbut, A. Mauro, and A. W. Clark. 1970. Effects of black widow spider venom on the frog neuromuscular junction. *Nature (Lond.).* 225:701–705.

Martin, A. R. 1955. A further study of the statistical composition of the end-plate potentiol. *J. Physiol. (Lond.).* 130:114–122.

Rice, S. O. 1944. Mathematical analysis of random noise. *Bell Tech. Syst. J.* 23:282–332.

Schick, K. L. 1974. Power spectra of pulse sequences, and implications for membrane fluctuations. *Acta Biotheor.* 23:1–17.

Segal, J. R., B. Ceccarelli, and W. P. Hurlbut. 1983. A novel use of Campbell's theorem to determine the amplitude, time course, and frequency of occurrence of miniature endplate potentials during protracted periods of intense secretion. *Biophys. J.* 41(2, Pt.2):136*a*. (Abstr.)

Sigworth, F. J. 1981. Interpreting power spectra from nonstationary membrane current fluctuations. *Biophys. J.* 35:289–300.

Simonneau, J., L. Tauc, and G. Baux. 1980. Quantal release of acetylcholine examined by current fluctuation analysis at an identified neuro-neuronal synapse of Aplysia. *Proc. Natl. Acad. Sci. USA.* 77:1661–1665.

Takeuchi, A., and N. Takeuchi. 1959. Active phase of frog's end-plate potential. *J. Neurophysiol.* 22:395–411.

Tauc, L. 1982. Nonvesicular release of neurotransmitter. *Physiol. Rev.* 62:857–893.

Valtorta, F., L. Madeddu, J. Meldolesi, and B. Ceccarelli. 1984. The receptor of α-latrotoxin is an externally exposed protein of the presynaptic membrane. *J. Cell Biol.* 99:124–132.

Verveen, A. A., and L. J. De Felice. 1974. Membrane Noise. *Prog. Biophys. Mol. Biol.* 28:189–268.

Weibel, E. R., and D. Paumgartner. 1978. Integrated stereological and biochemical studies on hepatocytic membranes. II. Correction of section thickness effect on volume and surface density estimates. *J. Cell Biol.* 77:584–597.

Wong, F., and B. W. Knight. 1980. Adapting bump model for eccentric cells of *Limulus*. *J. Gen. Physiol.* 76:539–557.